e-JSNM

e-JURNAL SAINS NUKLEAR MALAYSIA

e-NUCLEAR SCIENCE JOURNAL OF MALAYSIA

Volume 38 (Special Issue) 2026

A scientific journal by Malaysian Nuclear Agency

eISSN 2232-0946

eJURNAL
SAINS NUKLEAR MALAYSIA
VOL. 38(SPECIAL ISSUE) 2026
eISSN: 2232-0946

Jurnal Sains Nuklear Malaysia (JSNM, Nuclear Science Journal of Malaysia) is published in the months of June and December annually since 1982 by the Malaysian Nuclear Agency (formerly known as PUSPATI, UTN and MINT). This journal provides a platform for researchers, scientists and engineers (RSEs) to publish their research findings and reviews related to nuclear science and technology so that they can be shared with colleagues throughout the world.

As a means to internationalise JSNM, the Board of Editors welcomes scientific, technical and review articles written by members of the scientific community from home and abroad.

Previously a purely traditional printed journal, JSNM is now adapted and available in electronic form, in keeping with demands and rapid development of ICT. This adaptation also translates to ease of accessibility of JSNM for scientific communities as well as to facilitate knowledge sharing among RSEs.

On behalf of the Editorial Board of JSNM, we would like to acknowledge and thank the authors and referees for their significant contributions to the success of this journal and for embracing this new publication format.

Every effort has been made to trace and acknowledge all copyright holders, but if any have been inadvertently overlooked, the publishers would please to make the necessary arrangements at the first opportunity.

Publishing Office
Malaysian Nuclear Agency, Bangi,
43000 Kajang,
Selangor Darul Ehsan,
MALAYSIA
Tel : +6 03 8911 2000
Fax : +6 03 8911 2154

Website
http://jsnm.nuclearmalaysia.gov.my

TABLE OF CONTENTS

Jurnal Sains Nuklear Malaysia, 2026, 38(Special Issue): 1 – 9
ISSN: 2232-0946

YTTRIUM RECOVERY: A SELECTIVE LEACHING STRATEGY FROM FUSED XENOTIME

Roshasnorlyza Hazan*, Mimi Anisa Romli, Zakiah Zamri, Nur Hanisah Asri, Khaironie Mohamed Takip, Nur Aqilah Sapiee, Norhazirah Azhar, Wilfred Paulus, and Jacqueline Kones

Materials Technology Group (MTeG), Industrial Technology Division, Agensi Nuklear Malaysia, Bangi, 43000 Kajang, Selangor, MALAYSIA.
*Correspondence author: roshasnorlyza@nm.gov.my

ABSTRACT

This research investigates a selective leaching strategy aimed at efficient recovery of yttrium (Y) from fused xenotime in response to the increasing demand for this essential rare earth element (REE) in various high-tech applications. The development of selective leaching strategies is vital for the sustainable and economically viable production of Y. The proposed research adopts a hydrometallurgical approach, utilizing selective leaching to recover Y from fused xenotime while minimizing the dissolution of other matrix components, thereby simplifying separation processes. The leaching process requires careful control of several factors, including the selection of leaching agents (hydrochloric acid (HCl), nitric acid (HNO_3), sulfuric acid (H_2SO_4), and acetic acid), acid concentration, duration, temperature, and solid-to-liquid ratio, to optimize the recovery and selectivity of Y. The fused xenotime and the leachates were analyzed using X-ray fluorescent (XRF) techniques to determine the elements present in the samples. Experiments were conducted at room temperature for one hour with varying molarities of leaching agents; the maximum recovery for Y was found to be 79%, 61%, 58%, and 36% for leaching with 4 M HNO_3, 2 M HCl, 3 M acetic acid, and 1 M H_2SO_4, respectively. However, uranium (U) began to appear in the leachate at low concentrations (0.2 M) of H_2SO_4 and acetic acid and at 1.5 M of HNO_3 and HCl. Additionally, thorium (Th) began to be detected in the leachate after using 0.5 M H_2SO_4, 2 M acetic acid, 2 M HNO_3, and 6 M HCl. Therefore, it is recommended to use 1.5 M HNO_3 for leaching the fused xenotime, as this concentration can effectively prevent the dissolution of U and Th while still achieving a high recovery of Y (66%). Following the selective leaching stage, solvent extraction techniques can be utilized to further purify the Y-rich leachate and eliminate any residual contaminating metal ions that may have co-dissolved during the leaching process.

Keywords: Alkaline fusion; rare earth element (REE); recovery; selectivity; XRF

INTRODUCTION

In recognition of its special qualities as a rare earth element (REE), yttrium is in high demand on the international market. Furthermore, the aforementioned study aligned with Malaysia's Sustainable Development Goals (SDG) in several areas, including clean water and sanitation, affordable and clean energy, industry, innovation and infrastructure, and climate action (DOSM, 2019). Through the National Advanced Materials Technology Road Map 2021–2030, Malaysia aims to attract RM100 billion in investment from various investors by 2030, resulting in the creation of 4000 jobs and RM747.2 billion in revenue (MOSTI, 2022). This initiative also contributes to a specific goal in a flagship program for environmental and natural resource management as part of the Dasar Teknologi Nuklear Negara 2030 vision (Nuklear Malaysia, 2021). Furthermore, Wawasan Nuklear Malaysia for Nuclear Science and Technology is implementing strategic core number 1 to enhance industrial

competitiveness (MOSTI, 2023). Y provides excellent functionality in numerous green and high-tech components (Haxel et al., 2002). Some of the applications of yttrium are solid oxide fuel cells (SOFC) (Vasconcellos et al., 2006), superconductors (Basuki et al., 2020), chemically stable substrates, crucible materials for melting reactive metals, cutting tools, infrared windows, thermal barrier coatings, solid-state laser host materials, and catalyst support (Gribov et al., 2023). However, limited processing knowledge (Jordens et al., 2013), sustainability of locally produced yttrium in purity, and cost-effectiveness from the upstream sector up to its commercialization are the primary obstacles to yttrium's commercialization. Since Malaysia has abundant natural sources of amang and is rich in yttrium (27–41%), it could be utilized as the raw material for yttrium production (Amer et al., 2016 and Mohamed and Saleh, 2017) depending on its origin.

Yttrium separation and purification can be achieved through various methods, such as solvent extraction and precipitation. In a rich yttrium pregnant leach solution, 50–60% Y_2O_3 may be obtained in a single leaching process (Xaba et al., 2018). However, Y in nature coexist with the other REE gang, Th and U. Separating individuals became a major challenge for the industry. Therefore, selective leaching could facilitate the separation process by controlling the dissolution of Y and other elements. In this research paper, the efficient recovery of Y while minimizing the dissolution of other matrix components was studied.

MATERIALS AND METHODS

Materials

The xenotime ores were collected from Kinta Valley, Perak, Malaysia. Table 1 displays the major elements present in the xenotime ore and fused xenotime. Other chemicals, such as 37% HCl, 68% HNO_3, 98% H_2SO_4 and 99% acetic acid manufactured by Merck, Fisher Chemical, R&M Chemical, and HmbG Chemical, respectively, were analytical grade.

Table 1. Elemental composition of xenotime.

Element	Elemental composition (wt. %)	
	Ore	Fused
Rare Earth elements (REE)		
Y	21.98 ± 0.18	52.72 ± 0.32
Gd	1.374 ± 0.08	3.06 ± 0.24
Tm	ND	2.07 ± 0.58
Ho	0.66 ± 0.06	2.40 ± 0.01
Yb	5.57 ± 0.04	9.32 ± 0.34
Nd	1.96 ± 0.08	3.00 ± 0.57
Ce	1.79 ± 0.10	2.30 ± 0.55
Radioactive elements		
Th	0.45 ± 0.01	0.92 ± 0.19
U	0.38 ± 0.01	0.91 ± 0.08
Other elements	65.83 ± 0.10	23.29 ± .019

*ND = not detected

Selective Acid Leaching

Under predetermined ideal conditions, xenotime samples were fused from an earlier work with NaOH (Hazan et al., 2025). Subsequently, different acid molarities for acid-leaching parameters were analyzed to ascertain their optimal values for selective leaching of heavy rare earth elements (HREE). Each of the experiments was carried out in a closed system at room temperature (25 °C) for an hour. The leached product was thoroughly rinsed and filtered using deionized water. XRF was employed to analyze both the leachate and its solid residue. Only HREE, which solubilizes the leachate in the absence of thorium and uranium, will advance to the subsequent phase**.**

Analytical techniques

The elemental analysis was performed by XRF spectroscopy using EDX-7000 by Shidmadzu for both liquid and solid samples. All samples were prepared in triplicate to ensure repeatability. The data's uncertainty was documented according to the recommendations of the EDX-7000 program. The recovery of elements (R%) in leachate was calculated based on equation 1.

$$\%\ leaching\ recovery\ of\ REE = \frac{amount\ of\ element\ in\ leachate\ (g)}{initial\ amount\ of\ element\ in\ fused\ xenotime\ (g)} \times 100 \qquad (1)$$

RESULTS AND DISCUSSION

Effect of HCl Concentration on REE Recovery

The REE contents were measured at different HCl molarity acids. Figure 1 illustrates the recovery of rare earth elements (REE) after leaching fused xenotime using various concentrations of HCl. As may be seen in Figure 1(a, b, d), Y recovered 60% upon leaching between 1.5 M and 4 M HCl; Gadolinium (Gd) recovered 70% upon leaching with 1.5 M HCl; and Holmium (Ho) recovered ~58% upon leaching between 2 M and 4 M. Due to Y and Gd's increased solubility in slightly stronger acidic conditions, Y and Gd most likely showed higher leaching effectiveness in 1.5 M HCl than other REEs. However, the solubility of most REE decreased upon increasing the HCl molarity due to the development of stronger complexation and precipitation between REE and chloride into REE-chloride complexes. These conditions could limit the further dissolution of REE in the system. Other REEs may experience a maximum recovery of 28% thulium (Tm) upon leaching with 4 M HCl. Oversaturation and the common-ion effect were the causes of Tm's decreased dissolving ability. The common-ion effect is the result of an equilibrium when any of the reaction elements in the reaction are shared in the reacting system (Ayogu et al., 2020). Meanwhile, the recovery of Neodymium (Nd) keeps increasing upon leaching with 12 M HCl (Figure 1(c)). It was due to the greater solubility of Nd under strong acidic conditions.

Effect of HNO_3 Concentration on REE Recovery

Figure 2 shows the leaching recovery of fused xenotime using different HNO_3 concentrations. Figure 2 indicates that REE recovery was in equilibrium after a certain HNO_3 molarity. Notably, the highest Gd recovery of 97% was observed upon leaching with 1.75 M HNO_3. Gd likely had higher leaching in 1.75 M than other REE due to its greater solubility. The maximum Y recovery of 79% was observed when leaching with 4 M HNO_3. On the other hand, cerium (Ce) starts to recover with 6 M HNO_3 leaching. It means that Ce needs a higher acid concentration to increase proton activity to ensure higher dissolution efficiency. This experiment indicates that Ce and Yb were leached out using HNO_3. As compared to HCl leaching, both elements were detected. The results indicated that the HNO_3 was able to break down the fused xenotime structure more effectively and overcome the common-ion effect for Ce and Yb.

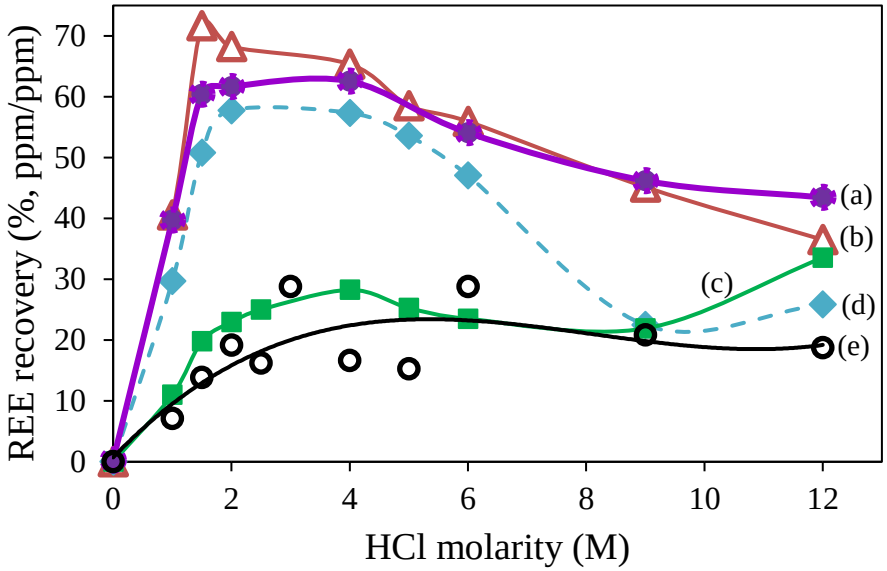

Figure 1 Effect of HCl concentration on REE recovery ((a) Y, (b) Gd, (c) Nd, (d) Ho, and (e) Tm after HCl leaching of fused xenotime

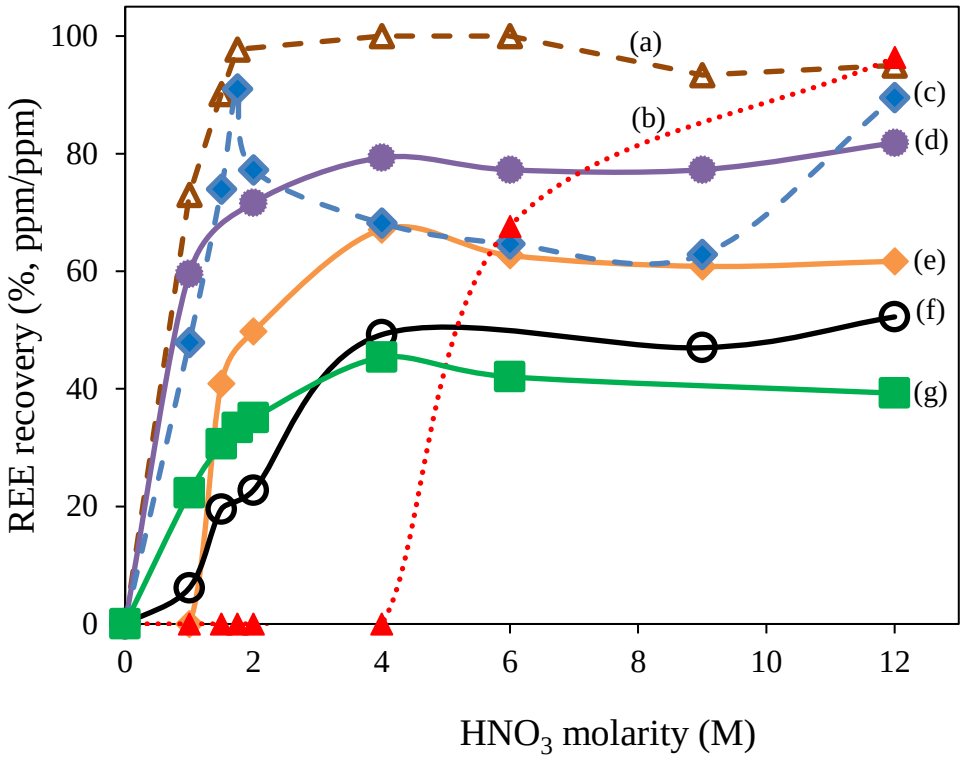

Figure 2 Effect of HNO_3 concentration on REE recovery ((a) Gd, (b) Ce, (c) Ho, (d) Y, (e) Yb, (f) Tm, and (g) Nd) after HCl leaching of fused xenotime.

Effect of H_2SO_4 Concentration on REE Recovery

The effect of different concentrations of H_2SO_4 on the leaching of fused xenotime was investigated from 0 M to 12 M H_2SO_4 and was shown in Figure 3. The recovery of most rare earth elements (REE) was lower than 40% when compared to that of another leaching agent. In this experiment, Y just recovered 50% between 0.5 M and 4 M H_2SO_4 leaching. REE likely had lower leaching recovery in H_2SO_4 due to its specific chemical behavior or complexation in fused xenotime. There was precipitate existing after the leaching process, and it can be seen in the H_2SO_4 leachate. This phenomenon was not preferred, as it will affect the solvent extraction stage in the future. It was the result of leached REE in H_2SO_4 tending to precipitate back in the leachate. In contrast, the recovery of Ce was 100% when leaching with 4 M to 6 M H_2SO_4. Therefore, H_2SO_4 is suitable to leach Ce from fused xenotime between 4 M and 6 M, as other REE recovery was low (10 to 50% recovery only). This finding suggests that H_2SO_4 was not suitable to leach REE from fused xenotime except for Ce.

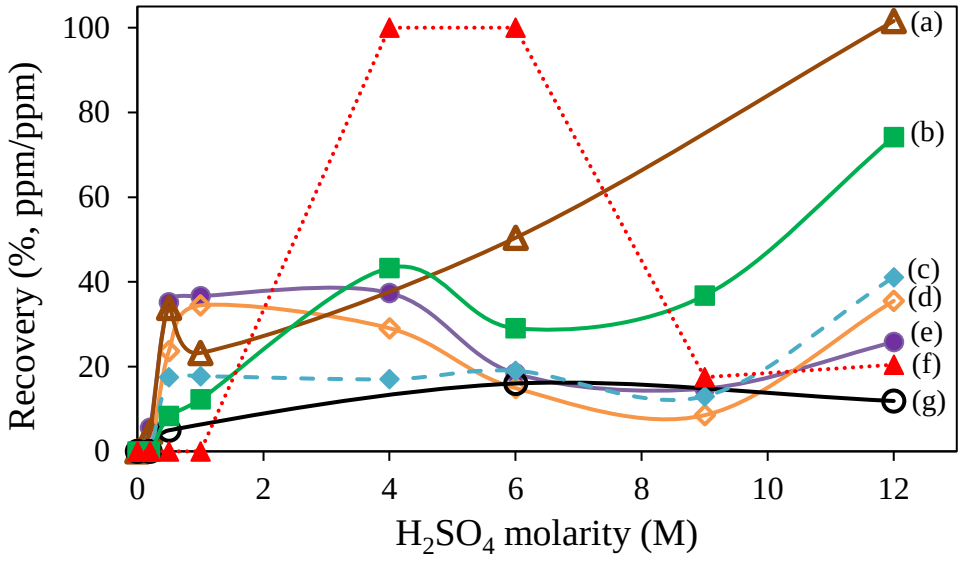

Figure 3 Effect of H_2SO_4 concentration on REE recovery ((a) Gd, (b) Nd, (c) Ho, (d) Yb, (e) Y, (f) Ce, and (g) Tm) after HCl leaching of fused xenotime.

Effect of Acetic Acid Concentration on REE Recovery

The leaching recovery results under various acetic acid molarities were shown in Figure 4. At 1 M acetic acid, Y just recovered 50%. Most REE recovery was low (<40%). In 2024, Zhang et al. reported that adding some acetic acid to the leaching process of aluminium (Al) could effectively reduce the REE losses. Such results could suggest that a small amount of acetic acid could assist the leaching process by controlling and selectively leaching the unwanted elements rather than being the major leaching agent. The leaching experiment was not continued for higher concentrations of acetic acid due to thorium (Th) and uranium (U) recovery starting at 2 M and 0.2 M, respectively, according to Figure 5. For REE, its leaching recovery was lower in acetic acid, as it is less reactive in acetic acid compared to Th and U. This phenomenon will be discussed further in the next section.

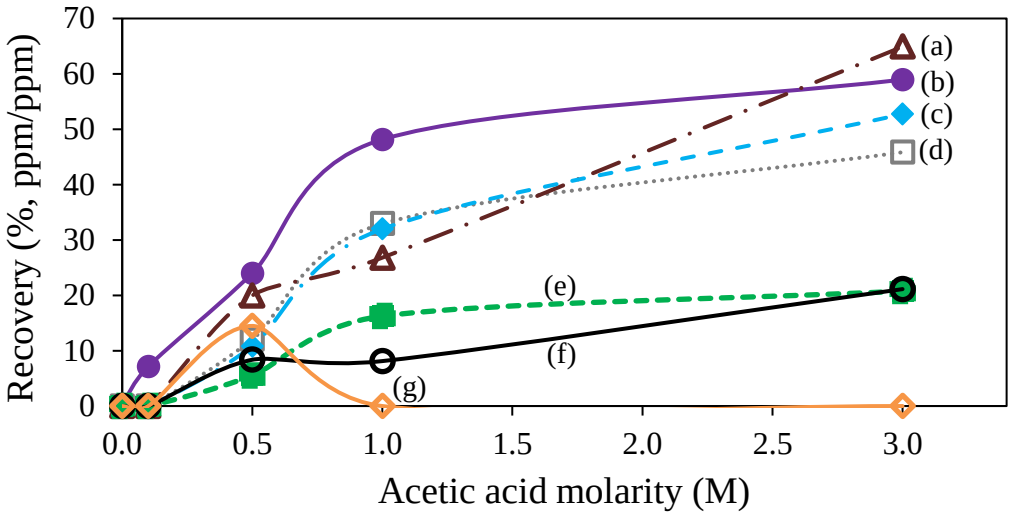

Figure 4 Effect of acetic acid concentration on REE recovery ((a) Gd, (b) Y, (c) Ho, (d) Dy, (e) Nd, (f) Tm, and (g) Yb) after HCl leaching of fused xenotime.

Effect of different acid concentrations on Th and U dissolution

The results of applying different acid concentrations on Th and U dissolution from fused xenotime are shown in Figure 5. The idea is to leach out REE into the leachate while preventing Th and U from dissolving into the leachate and maintaining both elements in the solid phase. The dissolution of U began to appear in the leachate at low concentrations (0.2 M) of H_2SO_4 and acetic acid and at 1.5 M of HNO_3 and HCl. Whereas, Th began to be detected in the leachate after using 0.5 M H_2SO_4, 2 M HNO_3, and 6 M HCl. This comparison reveals that Th and U have higher acid affinity in H_2SO_4, as both elements dissolve in H_2SO_4 at low concentrations. Th was not dissolved in acetic acid, as it needs higher acidity to break down its binding affinity.

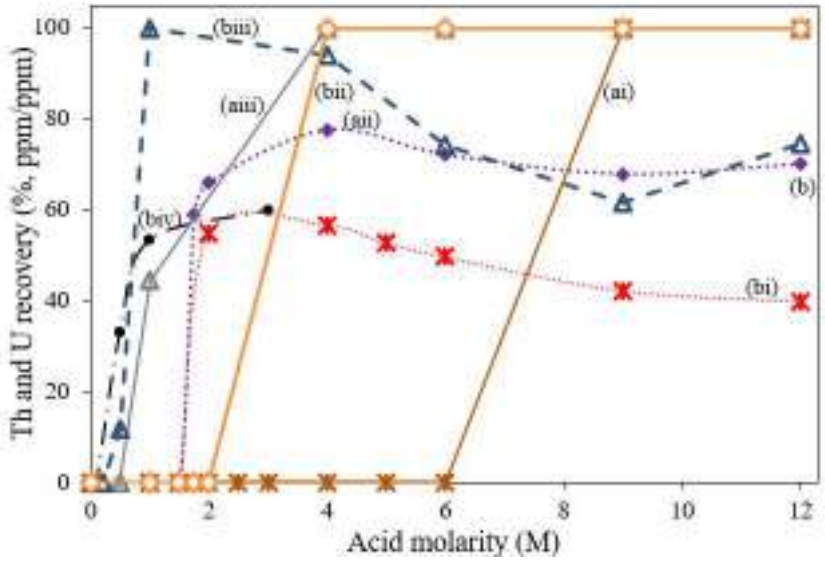

Figure 5 Effect of different acid concentrations on (a) Th and (b) U dissolution from fused xenotime using (i) HCl, (ii) HNO_3, (iii) H_2SO_4, and (iv) acetic acid.

This study reveals that maximum recovery for Y was found to be 79%, 61%, 58%, and 36% for leaching with 4 M HNO_3, 2 M HCl, 3 M acetic acid, and 1 M H_2SO_4, respectively. From this study, it is recommended to use 1.5 M HNO_3 for leaching the fused xenotime, as this concentration can effectively prevent the dissolution of U and Th while still achieving a high recovery of Y (66%). With this research, the fused xenotime, when properly fused and leached, can effectively recover REE in the leachate while preventing dissolution of Th and U to ensure the products are radioactively free.

For selective leaching, all elements offer some compelling insights into the underlying mechanisms of rare earth element leaching from a xenotime matrix. The general trend observed for elements was an initial increase in recovery with increasing acid molarity, followed by a peak, and then a decrease or levelling off at higher acid concentrations. This classic profile in acid leaching suggests a balance of several physicochemical processes. The initial increase in recovery (0 M to ~2 M acid) occurs at lower acid concentrations, as the primary mechanism is the protonation and dissolution of the rare earth compounds, likely present as oxides, hydroxides, or complex compounds within the fused xenotime matrix. The fused xenotime would have been liberated more because of acid attack due to structural changes from the fusion process. Acid solution provides H^+ ions that react with the mineral complexes, breaking down the crystal lattice within the fused xenotime and releasing the REE ions into the aqueous phase. The dissolution reaction can be generally represented as acid concentration increases, the availability of H^+ ions rises, driving the dissolution equilibrium forward and enhancing the kinetics of leaching, thus leading to higher recovery (Zhao et al., 2024).

The peak recovery is represented in the second stage by the optimal balance between sufficient acid concentrations for dissolution and other factors that might hinder recovery at higher concentrations (Maltrana and Morales, 2023). At this point, the rate of dissolution is maximal, and the rare earth ions are stable in solution, likely as hydrated ions or simple chloride complexes. In the last stage of acid leaching, a decrease or levelling off in recovery (above ~4 M acid) occurs due to the decline in REE recovery at higher acid concentrations. This is a critical observation that can be attributed to several factors, such as the common ion effect or salting out, the formation of less soluble chloride complexes, and the kinetics of precipitation. In common ion effector salting out, at very high ionic strengths (high acid concentration), the activity coefficients of the dissolved REE ions can decrease significantly. These decreases can lead to a "salting out" effect, where the solubility of the rare earth solutions (or other less soluble REE species) in the highly concentrated acid solution decreases, potentially causing precipitation. Whereas the formation of less soluble chloride complexes happens at very high concentrations, REE ions might form highly stable, but less soluble, complex species with chloride ions (for example, anionic chloro-complexes). The formation of these species could shift the equilibrium away from the free, highly soluble REE^{3+} ions, leading to reduced recovery if these complexes are less stable or prone to precipitation under these conditions. In addition, in kinetics of precipitation (Romano et al., 2025), the very high concentration of hydrogen and chloride ions might also favour the formation of new, less soluble phases or a shift in the reaction equilibrium that precipitates some of the dissolved REEs.

However, Nd shows a moderate recovery, while Ho and Tm exhibit significantly lower recoveries. This difference is mechanistically important. Rare earth elements have slightly different chemical properties due to their varying ionic radii and electronic configurations (lanthanide contraction). These differences affect their solubility, complexation, and chemical binding in the matrix. Some REE solutions might be inherently less soluble at high acid concentrations than others. Also, multiple elements' existence would form complexes of varying stability with chloride ions, influencing their speciation and solubility in concentrated acid. The initial distribution and chemical binding of these multiple elements within the fused xenotime might also vary and affect the leaching process. This phenomenon would impact elements released in the aqueous phase during leaching. Some complexes might be more structurally integrated or exist as different mineral phases (Muhammad et al., 2025).

This finding provides valuable insights for optimizing the single-stage acid selective leaching process. Understanding these mechanistic behaviours is key to developing more efficient and environmentally viable hydrometallurgical processes, aligning with the goal to enhance yttrium supply locally.

CONCLUSION

In conclusion, the maximum recovery for Y was determined to be 79%, 61%, 58%, and 36% for leaching with 4 M HNO_3, 2 M HCl, 3 M acetic acid, and 1 M H_2SO_4, respectively. Utilizing 1.5 M HNO_3 for leaching fused xenotime is advisable, since this concentration efficiently inhibits the dissolution of U and Th while attaining a substantial recovery of Y (66%).

ACKNOWLEDGEMENTS

The authors really appreciate the support from the Malaysian Nuclear Agency through NM-R&D-24-09.

REFERENCES

Amer, T. E., Abdellah W. M., Abdel Wahab G. M., and El-Shahat M. F., (2016). Selective Separation of Yttrium and Cerium (IV) from the Prepared Abu Hamata Lanthanides Cake, *Chem. Biomol. Eng*., 1(26-31).

Ayogu, P. C., Ezugwu, M. I., and Eze, F. I., (2020). Principle of Common-ion Effect and its Application in Chemistry: a Review, *J. Chem. Lett*., 1(77-83).

Basuki, K. T., Arifudin, R., Pusparini, W. R., and Saputra, A., (2020). Dysprosium (Dy) Separation from Yttrium Concentrate in Nitric Acid Solution Using Aliquat 336 Solvent, *Key Engineering Materials*, 840(573-579).

DOSM. (2019). Sustainable Development Goals (SDG) Indicators Malaysia, Department of Statistics, Malaysia. ISSN: 2682-9355.

Haxel, G. B., Hedrick, J. B., and Orris, G. J., (2002). Rare Earth Elements—Critical Resources for High Technology, US Geological Survey, fs(087-02).

Hazan, R., Kamarudin, N. A., Asri, N., Sapiee, N. A., Mohamed Takip, K., Paulus, W., Azhar, N., and Kones, J., (2025). Phosphate removal and yttrium recovery from xenotime mineral via alkaline fusion, *IOP Conf. Series: Mater. Sci. Eng.*, 1326(012006).

Gribov, P. A., Sidelnikov, A. A., Belosludov, R. V., and Matvienko, A. A., (2023). Synthesis of Nanocrystalline Yttrium Oxide and Evolution of Morphology and Microstructure during Thermal Decomposition of $Y_2(C_2O_4)_3{\cdot}10H_2O$, *Ceramics*, 6(16-29).

Jordens, A., Cheng, Y. P., and Waters, K. E., (2013). A review of the beneficiation of rare earth element bearing minerals, *Mineral Engineering*, 41(97-114).

Maltrana, V., and Morales, J., (2023). The Use of Acid Leaching to Recover Metals from Tailings: A Review, *Metals*, *13*(11).

Mohamed, M. F., and Saleh, M. E., (2017). Recovery of Yttrium and Dysprosium from the Rare Earths Concentrate, Southwestern Sinai, *Inorg. Chem. Ind. J*., 12(118).

MOSTI. (2022). National Advanced Materials Technology Roadmap 2021-2030. Ministry of Science, Technology & Innovation (MOSTI), Malaysia.

MOSTI. (2023). Dasar Teknologi Nuklear Negara 2030. Ministry of Science, Technology & Innovation (MOSTI), Malaysia. ISBN 978-967-2741-10-7.

Muhammad, N. N. N., Muna, N. A., Mohd Yunus, M. Y., Kassim, K., Jamion, N. A., Megat Hanafiah, M. A. K., Ghazali, N. F., and Yong, S. K., Advances in the Development of Leaching Agents for Assisting Phytoremediation of Rare Earth Elements: A Review, *Malaysian Journal of Chemistry*, 27(27-50).

Nuklear Malaysia. (2021). Wawasan Nuklear Malaysia 2030. Agensi Nuklear Malaysia. ISBN 978-967-2706-05-2.

Romano, P., Rahmati, S., Adavodi, R., Clementini, G., Gallo, F., and Vegliò, F. (2025). Study of the kinetics and mechanisms of rare earth elements leaching from end-of-life NdFeB magnets through Hydro-Nd process, *Separation and Purification Technology*, 356(129850).

Vasconcellos, M. E., Rocha, S. M. R., Pedreira, W. R., Queiroz, C. A. S., and Abrão, A., (2006). Enrichment of yttrium from rare earth concentrate by ammonium carbonate leaching and peroxide precipitation, *J. Alloys Compounds*, 374(405-407).

Xaba, S. M., Nete, M., and Purcellet, W. (2018). Concentration of rare earth elements from monazite by selective precipitation, *IOP Conf. Series: Mater. Sci. Eng.*, 430(012006).

Zhang, Y. Z., Chen, J., Zhang, H., Gong, S., Xiao, Y., and Huang, L. (2024). Reducing rare earth loss by adding acetic acid in the aluminum removal process of rare earth leaching solution, *J. Clean. Prod.,* 435(140537).

Zhao, D., Sun, H., Peng, T., Zeng, L., and Wu, M., (2024) The acid-leaching process and structural changes of lizardite, chlorite and talc in sulfuric acid medium, *Clay Minerals*, 59(298-309).

Jurnal Sains Nuklear Malaysia, 2026, 38(Special Issue): 10 – 17
ISSN: 2232-0946

SCRUBBING STUDY ON RARE EARTH LOADED ORGANIC FROM EXTRACTION PROCESS OF YTTRIUM

Nur Aqilah. Sapiee*, Roshasnorlyza Hazan, Khaironie Mohamed Takip, Wilfred Sylvester @ Paulus, Jacqueline Kones and Norhazirah Azhar

Material Technology Group, Nuclear Agency,
43000 Kajang, Selangor, Malaysia
*Correspondence author: nuraqilah@nm.gov.my

ABSTRACT

Separation process of rare earth elements is normally accomplished using solvent extraction that consists of extraction, scrubbing stage and stripping stage. Since the separation of rare earth elements is difficult due to their chemical similarities, improvement of the process need to be done to increase separation factors and to reduce chemical consumption thus will reduce chemical waste. This study focused on scrubbing stage for extraction of yttrium from Malaysian Xenotime. The objective of this study is to find the best scrubbing agent in order to remove inorganic element from loaded organic phase as much as it can. Three different media were chosen as scrubbing agent which is deionized water, nitric acid and ammonium nitrate to scrub calcium, sulfur and chlorine produced from rare earth loaded organic solution. Results from X-Ray Fluorescence (XRF) shows that 70°C deionized water with contact time of 10 minutes have a tendency to scrub most sulfur (15.2 ppm), chlorine (0.56 ppm) and calcium (26.2 ppm)from loaded organic solution.

Keyword: Scrubbing, Rare Earth, Xenotime, Solvent Extraction , XRF.

INTRODUCTION

Rare earth elements (REEs) have growing as a worldwide demand in recent years. After many years of research and development, rare earth elements had proved their advantages in green technologies such as next generation wind turbine and electric vehicles. Rare earths also used in the manufacture of optical sensors (yttrium), ceramic (lanthanum), permanent magnets (neodymium) and catalyst in oil refining (lanthanum). More recently, the term ‘rare earths’ has been used to designate the element themselves. Scandium and yttrium tend to occur in the same ore deposits as lanthanides and exhibit similar chemical properties (Balaram et al., 2019).

In Malaysia, major source of rare earth in mineral is xenotime (heavy rare earth) and monazite (light rare earth). Xenotime (YPO_4) is classified as radioactive mineral. Malaysian xenotime had been assumed consist of 30% of yttrium and 40% rare earth. Xenotime is fused with sodium hydroxide at 350°C to help phosphate removal from the rare earth more efficient compared than other route such as acid digestion (Roshasnorlyza et al., 2025). A part of the precise leaching process, the leach solution usually contain dissolved impurities such as chlorine, phosphorus and calcium which are removed by precipitation before proceeding to solvent extraction to separate rare earths.

Solvent extraction begins by separating different group of rare earths from leach solution. Individual rare earths are difficult to separate from each other due to their similar physical and chemical properties. Separation processes based on solvent extraction and ion-exchange technique had been developed to produce high purity single rare earth solutions or compounds (Peiqiang Fan et al., 2023) (Youssef et al., 2023). Solvent extraction is used as commonly the most appropriate commercial technology for separating rare earths (Feng Xie et al., 2014) (Abreu et al., 2014) (Hiskeya et al., 2018) (Wu et al., 2018) due to the need to be able to handle larger volumes of leach solution. Also, solvent extraction is being developed as environmental friendly technique since there is no use of high temperature compared than pyrometallurgy studies.

Separation and purification of rare earth using solvent extraction processes have been reviewed. There are four classes of extractant, namely as cation exchangers, solvation extractants, anion exchangers and chelating extractants that have been utilized for separating rare earths . In this study, cation exchanger which is di-ethylhexyl phosphoric acid (DEHPA) is used as extractants for separation of rare earth in kerosene and aqueous chloride solution. DEHPA can extract 100% of thorium at low concentration (Nur Aqilah et al, 2019) but because of the distribution coefficient and separating factors that lies strongly in the organic solution, it is difficult to strip the loaded organic. Therefore, scrubbing technique is proposed to remove inorganic co-extracted element in order to make stripping become more efficient.

Several investigations have been reported in the literature to study the behavior of scrubbing technique towards removal of inorganic element. Jorjani et al., 2012 studied the behavior of loaded organic phase (from loaded Tri-Butyl Phosphoric Acid, TBP) that had been scrubbed with hot deionized water and ammonium nitrate. The results showed that three stages of scrubbing with a phase ratio (Va/Vo) of five removed about 80%, 30%, 27%, and 15% of Ca, Mg, Fe, and P, respectively, from loaded TBP, while less than 9% of total REEs was lost.

The extraction of yttrium from Xenotime is carried out with DEHPA in kerosene. In this study, the form of yttrium and rare earth oxalate is produced after precipitation of leached solution from Alkaline Fusion of Malaysian Xenotime (Meor Yusoff MS et al., 2015). The pregnant liquor or rare earth loaded organic with DEHPA is then scrubbed with deionized water, nitric acid and ammonium nitrate.

MATERIALS AND METHOD

Preparation of pregnant liquor

The sample used in this study was prepared from alkaline fusion process of xenotime obtained from the stockpile of Nuklear Malaysia where sodium hydroxide pellets is used to mix with xenotime and fused in furnace for 350°C. Washing and leaching process is introduced as previous study (Meor Yusoff MS et al., 2015) and mixed rare earth oxalate is obtained. Mixed rare earth oxalate is then dissolved in 3M hydrochloric acid for it has optimum molarity for yttrium's extraction as Figure 1.

The extractants used for two stage extraction process were Diethylhexyl Phosphoric Acid (DEHPA), which was from Sigma-Aldrich. DEHPA is used without further purification. Kerosene, which was used as a diluent, was supplied by LabChem. Deionized water and hydrochloric acid (from RCI Labscan) is used in all the experiments for aqueous solutions. Nitric acid (from RCI Labscan) and ammonium nitrate (from Sigma-Aldrich) were used as scrubbing agent. The organic solutions from this

extraction process were called rare earth loaded organic or pregnant liquor and were analyzed by Energy Dispersive X-Ray Fluorescence (EDXRF), Shimadzu EDX-7000 model as Table 1.

Table 1: Concentration of organic element and inorganic element in rare earth loaded organic

Organic	Y	Gd	Dy	Ho	Er	Tm	Yb
Concentration (ppm)	52,310	363.9	3,540	1,320	3,350	739.0	6530

Inorganic	P	Ca	Na	Si	S	Cl	Mg
Concentration (ppm)	125,190	1970	129	133	2080	7010	41

Scrubbing of rare earth loaded organic

This study were conducted with three different scrubbing agent which is deionized water, nitric acid (from RCI Labscan) and ammonium nitrate from Sigma-Aldrich to remove undesirable loaded elements such as magnesium, sodium, chlorine, calcium, sulfur, iron and phosphorus. Rare earth loaded organic and scrubbing agent (aqueous) were mixed in a beaker with magnetic stirrer speed at scale two (IKA MAG). The concoction is transferred into a conical separating funnel when the mixing is completed, for two-phase separation. Then, the aqueous phase is used for analysis. The elements in aqueous phase (chlorine, calcium and sulfur) were analyzed by Energy Dispersive X-Ray Fluorescence (EDXRF), Thermo Scientific QUANT'X model. Parameters studied at this stage were different type of scrubbing media which consist of variable of concentration.

RESULTS AND DISCUSSION

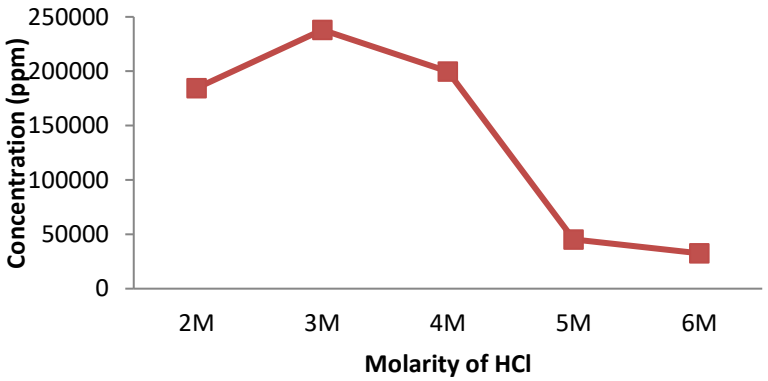

Figure 1: Concentration of extracted yttrium with different hydrochloric acid molarity.

The results are shown in Figure 1. The concentration of extracted yttrium decreases rapidly as the molarity of HCl increases up to 3 M. Beyond this point, the concentration of yttrium rises, possibly due to the availability of more extraction sites for yttrium. However, further increases in HCl molarity do not lead to any significant improvement in the extraction percentage. Overall, the highest concentration of extracted yttrium is observed at 3 M HCl.

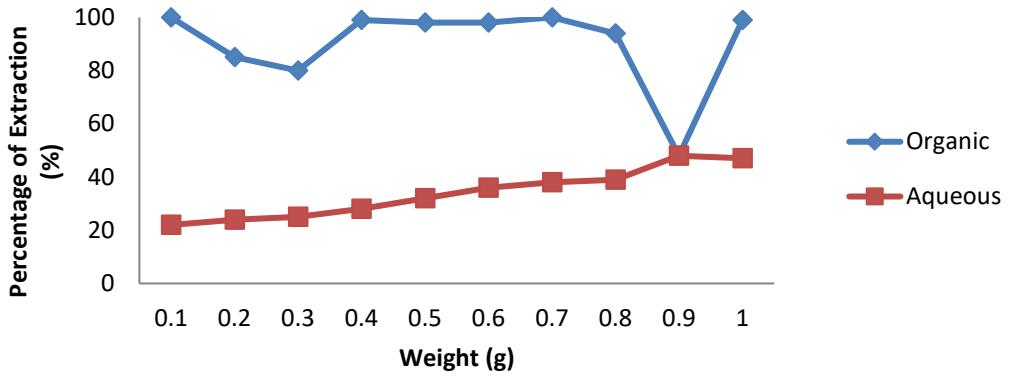

Figure 2: First stage extraction behavior of yttrium as a function of rare earth oxalate weight, contact time: 15 minutes, phase ratio: 1:1

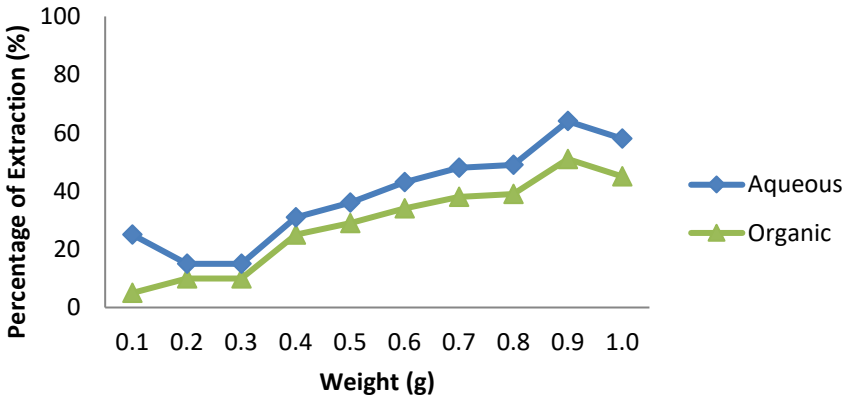

Figure 3: Second stage extraction behavior of yttrium as a function of rare earth oxalate weight, contact time: 15 minutes, phase ratio: 1:1

Figures 2 and 3 illustrate the behavior of yttrium extraction during the first and second stages after the pregnant liquor was produced. The results indicate that the percentage of extraction increases with the weight of rare earth oxalate. In the second stage of extraction, however, the percentage of extraction with 1.0 gram of rare earth oxalate shows a slight decrease, likely due to the limited availability of extraction sites for yttrium. Therefore, 1.0 gram of rare earth oxalate is identified as the optimum amount for yttrium extraction when using 30% DEHPA.

Scrubbing of rare earth loaded organic

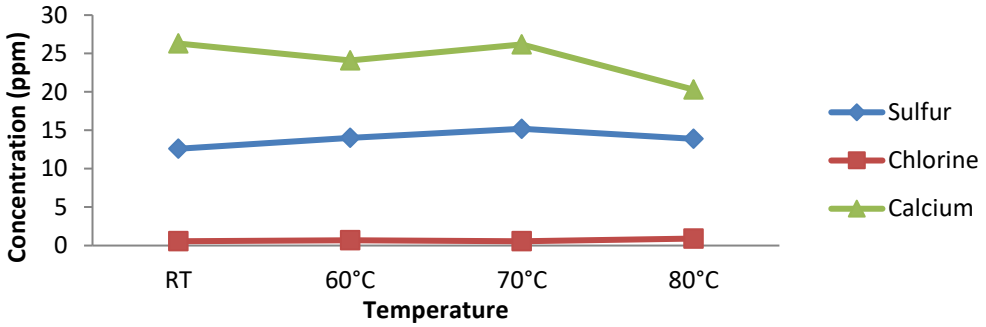

Figure 4: Effect of deionized water to rare earth loaded organic on the removal of inorganic elements.

Figure 4 shows that deionized water at 70 °C can scrub the highest amounts of sulfur (15.2 ppm), chlorine (0.56 ppm), and calcium (26.2 ppm) compared to room temperature, 60 °C, and 80 °C deionized water. The concentrations of sulfur and calcium increase as the temperature rises from room temperature (RT) to 70 °C. In contrast, chlorine removal is more effective at 80 °C, where a greater amount is scrubbed from the rare earth–loaded organic phase. These results were obtained after 10 minutes of contact time with an aqueous-to-organic ratio of 1:1.

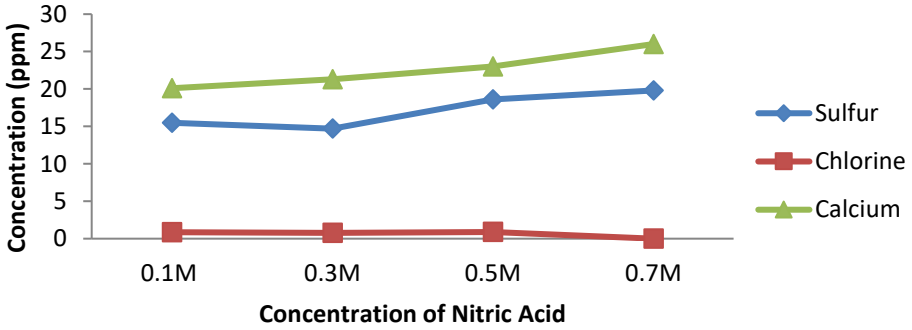

Figure 5: Effect of nitric acid to rare earth loaded organic on the removal of inorganic elements

Figure 5 shows that 0.7 M nitric acid, used as a scrubbing agent, effectively removes sulfur and calcium from the loaded organic phase, with concentrations of 19.8 ppm and 26.0 ppm respectively after 10 minutes of contact time at an aqueous-to-organic ratio of 1:1. For chlorine, the concentration decreases slightly, from 0.89 ppm at 0.5 M nitric acid to 0.00 ppm at 0.7 M.

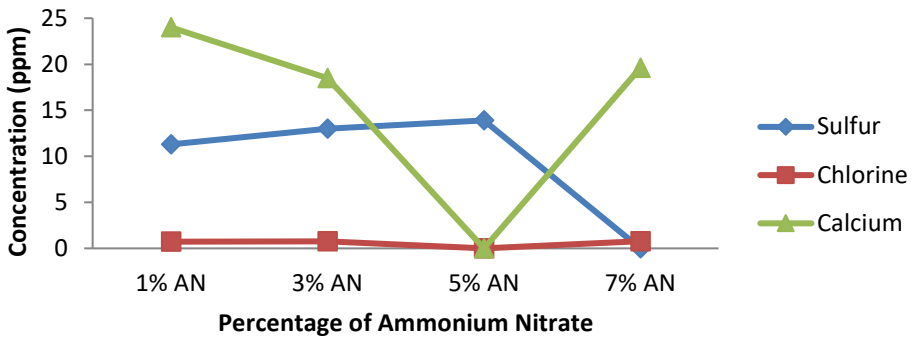

Figure 6: Effect of ammonium nitrate to rare earth loaded organic on the removal of inorganic elements

Figure 6 shows that the concentrations of sulfur and calcium increase rapidly with the percentage of aqueous solution, reaching their highest values at 3% ammonium nitrate after 10 minutes of contact time with an aqueous-to-organic ratio of 2:1. Beyond this point, the concentrations of chlorine and calcium decrease sharply at 5%, likely due to fewer available sites on the scrubbing agent to remove these elements. For chlorine, the concentration rises slightly from 0.73 ppm at 1% ammonium nitrate to 0.76 ppm at 3%, before dropping to 0.00 ppm at 5%.

CONCLUSION

This study proved that yttrium can be extracted from Malaysian Xenotime by extraction using DEHPA (30%) in hydrochloric acid solution. Scrubbing of the rare earth loaded organic phase to remove inorganic (impurities) were performed using deionized water, nitric acid and ammonium nitrate. Hot deionized water with 70°C scrub most sulfur (15.2 ppm), chlorine (0.56 ppm) and calcium (26.2 ppm) compared than other media.

ACKNOWLEDGMENTS

This research received support from the Malaysian Government for DSTIN FP0214D052: Development of Innovative Nuclear Reactor Technology (With The Spin-Off) Based on Thorium (Sub Project 2.1: Production of Nuclear-Grade Thorium and Uranium From Local Sources for Reactor Fuel).

REFERENCES

Abreu, R. D., & Morais, C. A. (2014). Study on separation of heavy rare earth elements by solvent extraction with organophosphorus acids and amine reagents. *Minerals Engineering*, *61*, 82–87. https://doi.org/10.1016/j.mineng.2014.03.003

Balaram, V. (2019). Rare earth elements: A review of applications, occurrence, exploration, analysis, recycling, and environmental impact. *Geoscience Frontiers*, *10*(4), 1285–1303. https://doi.org/10.1016/j.gsf.2018.12.005

Feng, P., Wenjie, Z., Xion, T., Xian, X., Ruiqi, X., Qiang, S., Yunpeng, D., & Yang, C. (2023). Separation and purification of light rare earth elements from chloride media using P204 and Cyanex272 in sulfonated kerosene under non-saponification conditions. *Physicochemical Problems of Mineral Processing*, *59*(5). https://doi.org/10.37190/ppmp/172444

Hiskeya, J. B., & Coppb, R. G. (2018). Recovery of yttrium and neodymium from copper pregnant leach solutions by solvent extraction. *Hydrometallurgy*, *177*, 21–26. https://doi.org/10.1016/j.hydromet.2018.02.010

Jorjani, E., & Malek, S. (2012). The production of rare earth elements group via tributyl phosphate extraction and precipitation stripping using oxalic acid. *Arabian Journal of Chemistry*, *28*(S2).

Meor Yusoff, M. S., Khaironie, M. T., Nursaidatul, K., Ahmad Khairulikram, Z., & Nuraqilah, S. (2015). An alternative alkaline fusion process for the production of heavy rare earth, thorium, uranium and phosphate from Malaysian xenotime. *Recent Advances in Environment, Ecosystem and Development*, 163–167.

Nur Aqilah, S., Khaironie, M. T., Roshasnorlyza, H., Ahmad Khairulikram, Z., & Wilfred, P. (2019). Extraction of thorium from Malaysian xenotime for preparation of nuclear grade thorium. *AIP Conference Proceedings*, *2068*(1), Article 020012. https://doi.org/10.1063/1.5089311

Roshasnorlyza, H., Nurhusnina Akma, K., Nurhanisah, A., Nur Aqilah, S., Khaironie, M. T., Wilfred, P., Norhazirah, A., & Jacqueline, K. (2025). Phosphate removal and yttrium recovery from xenotime mineral via alkaline fusion. *IOP Conference Series: Materials Science and Engineering*, *1326*(1), Article 012006. https://doi.org/10.1088/1757-899X/1326/1/012006

Wu, S. X., Wang, L. S., Zhang, P., El-Shall, H., Moudgil, B., Huang, X. W., Zhao, L. S., Zhang, L. F., & Feng, Z. Y. (2018). Simultaneous recovery of rare earths and uranium from wet process phosphoric acid using solvent extraction with D2EHPA. *Hydrometallurgy*, *175*, 109–116. https://doi.org/10.1016/j.hydromet.2017.10.021

Xie, F., Zhang, T. A., Dreisinger, D., & Doyle, F. (2014). A critical review on solvent extraction of rare earth from aqueous solution. *Minerals Engineering*, *56*, 10–14. https://doi.org/10.1016/j.mineng.2013.10.021

Youssef, E. O., Sami, V., Emile, S. M. M., Markku, L., Eveliina, R., & Katri, L. (2023). The recent progress of ion exchange for the separation of rare earths from secondary resources – A review. *Hydrometallurgy*, *218*, Article 106047. https://doi.org/10.1016/j.hydromet.2023.106047

Jurnal Sains Nuklear Malaysia, 2026, 38(Special Issue): 18 – 24
ISSN: 2232-0946

RECOVERY OF CERIUM, NEODYMIUM AND LANTHANUM FROM MALAYSIAN MONAZITE USING OXIDATION AND SELECTIVE PRECIPITATION METHOD

Jacqueline Kones*, Roshasnorlyza Hazan, Khaironie Mohamed Takip and Nur Aqilah Sapiee

Industrial Technology Division, Agensi Nuklear Malaysia, Bangi,
43000 Kajang, Selangor, Malaysia.
*Correspondence author: jacqueline@nm.gov.my

ABSTRACT

This study utilises a mixture of rare earth elements obtained from the Malaysian monazite through a series of processes from digestion to separation of non-radioactive and radioactive elements. The non-radioactive elements are the mixture of rare earth elements, mainly cerium, neodymium, and lanthanum. It is possible to separate cerium from other elements due to its ability to form +3 and +4 oxidation state compared to others. Therefore, the objective of this study was to compare the effectiveness of nitric acid HNO_3 and hydrochloric acid (HCl) as dissolution media for the separation of cerium from mixed rare earth hydroxide concentrates. The oxidation using nitric acid media was found to be incomplete hence leading to poor separation. 2 M HCl was proven to be more effective, yielding a cerium concentrate of approximately 71.2% purity. The remaining neodymium and lanthanum were separated through selective precipitation and the products obtained were analysed using Energy Dispersive X-ray Fluorescence (ED-XRF).

Keyword: Rare earth elements, cerium, neodymium, lanthanum.

INTRODUCTION

Rare earth elements (REEs) can be found naturally in the earth's crust. In Malaysia, it can be retrieved from the heavy mineral sand from processed tin tailing like xenotime and monazite. Other than that, REEs can also be obtained from adsorption clay minerals. Each source contains certain groups of elements, for example xenotime has more yttrium (Y) followed by heavy rare earth (HREE) and some light rare earth elements (LREE). Monazite, on the other hand, contains more LREEs namely cerium, neodymium, lanthanum, and praseodymium with presence of some HREEs.

In mineral processing, separation is a technique to isolate the substance of interest from others by using suitable techniques. For example, phosphate in monazite was removed using alkali digestion process. Separation is crucial as it facilitates the separation and concentration of the elements before extraction and purification can be done. The purpose to do extraction and purification is to obtain the highest concentration of the element of interest by minimising the presence of other elements. RE separation is commonly performed using the selective precipitation method. It means the desired elements will be removed by forming precipitate at a certain pH level. This method was used to separate REEs from thorium and uranium that are also present in monazite. After the REEs were concentrated, each REE can be separated too.

Another way that can be done to separate REE is to manipulate the property of the oxidation state. REEs generally have the oxidation state of +3 but in the case of cerium, it can also form +4 oxidation state. This is because, Ce has four valence electrons while others have three. The distinct oxidation state of Ce^{4+} allows for selective separation from trivalent REEs (Vapnik et al., 2025). It is important

to remove Ce from the mixed RE compound first before other elements can be purified because the presence of Ce will interfere with the purity of the final products (McNeice, 2018).

Oxidation of Ce can be done by reacting the mix rare earth solution with oxidising agent. Some oxidising agents that can be used are such as potassium permanganate ($KMnO_4$), hydrogen peroxide (H_2O_2), and sodium hypochlorite (NaOCl). Among these oxidants, $KMnO_4$ was found to be the most suitable to oxidise Ce (III) to Ce (IV) since H_2O_2 and NaOCl usually will decompose rapidly prior to reacting with Ce (III) (Sauber, 2018 & Morais et al, 2003). The oxidation of Ce (III) to Ce (IV) using $KMnO_4$ in acidic media is a robust method for high-purity separation, provided pH is strictly controlled to prevent manganese dioxide interference (Suyanti et al., 2025). Other than that, air oxidation method can also be done by drying the $RE(OH)_3$ cake obtained through precipitation RE in sulphate solution with NaOH at 120 °C (Rice, 1959). Oxygen at high temperature will oxidise Ce (III) (Formiga, & Morais, 2016).

For this study, the $RE(OH)_3$ used contains mixtures of Ce, Nd, La, Pr, some HRE, and other elements. This study aims to separate Ce mixed $RE(OH)_3$ by using two different acidic media, that is nitric acid (HNO_3) and hydrochloric acid (HCl) followed by separation of Nd and La through selective precipitation.

METHODS

$RE(OH)_3$ used in this study was obtained from Malaysia monazite through alkali digestion process. Finely ground monazite was digested with sodium hydroxide solution, then washed with hot water to remove trisodium phosphate that was formed. The hydrous monazite cake then reacted with concentrated hydrochloric acid solution for leaching process. After that, thorium and uranium elements were separated by conducting selective precipitation using ammonia solution at pH 5.8. The remaining elements in the filtrate was finally obtained as $REE(OH)_3$ by continuing the precipitation with excess ammonia. It contains mixtures of Ce, Nd, La, Pr, some HRE, and other elements.

a. Oxidation of Ce (III) in nitric acid.

Dried $RE(OH)_3$ was slowly added into concentrated nitric acid and heated until it fully dissolved. Water was added to dilute the acidic liquid, producing a yellow coloured solution. $KMnO_4$ solution was prepared by dissolving $KMnO_4$ into water. This solution was then added into the acidic solution. Solution of Na_2CO_3 was then added to precipitate Ce (IV) until pH 5. The solid compound formed was filtered while the remaining elements in the acidic solution were then precipitated by adding ammonia solution until pH 8. The solid compounds formed were dried and analysed using ED-XRF for their elemental content.

b. Oxidation of Ce (III) in hydrochloric acid.

Dried $RE(OH)_3$ was dissolved in hydrochloric acid with concentrations of 2 M and 37 % (v/v) until it was fully dissolved and then diluted with water for dilution. The pH of the acidic solutions was adjusted to pH 3 by adding Na_2CO_3 before a solution of $KMnO_4$ was added slowly. The pH of the reaction was maintained at pH 3 – 5 by adding more Na_2CO_3 when it dropped below pH 3. Addition of $KMnO_4$ was ceased only after the purple colour did not disappear. The solid compound formed was filtered and the remaining elements in the filtrate were precipitated with ammonia. The precipitated elements were dried and analysed using ED-XRF and X-ray diffraction (XRD).

c. Separation of Nd and La.

For this step, Nd and La remaining in the nitric acid solution were separated by adding NH_4OH solution until pH 7.5. The precipitated $Nd(OH)_3$ concentrate was filtered and washed followed by drying. More NH_4OH then added into the filtrant to retrieve La until no further precipitation was observed at around pH 10.30. Slurry of $La(OH)_3$ obtained was filtered, washed and dried. Both dried precipitates obtained were analysed by using ED-XRF.

RESULTS AND DISCUSSION

Monazite contains more cerium followed by neodymium, lanthanum and praseodymium. These are also known as the light RE elements. Other REEs that were detected are dysprosium and thulium. Thorium and uranium were also detected, and it can be separated by using the selective precipitation at pH-5.8 that the remaining elements were retrieved by adding ammonia solution in excess until no more precipitation observed. Separating the REEs is one way to increase the concentration of the elements individually. This will enable the enhancement of the extraction process as few elements were present in the mixture. $RE(OH)_3$ obtained previously will need to be dissolved in acidic media – for this study, nitric acid and hydrochloric acid were selected. Separation of Nd and La can be done after Ce was isolated.

a. Nitric acid as dissolution medium.

Dissolving $RE(OH)_3$ in HNO_3 was demonstrated in some reports (Wai, 2018; Purwani & Trinopiawan, 2019). The method used for this study was adapted from method by (Wai, 2018) in which the separation of cerium was done in two stages. In the first stage, some of cerium was reported to form a solid state after dilution of the acidic solution. As for the second stage, it happens after the reaction with potassium permanganate in excess followed by the addition of sodium carbonate. The filtrate remained then proceed to the next steps for the separation of the neodymium by continuing adding Na_2CO_3 solution until pH 8. Cerium was expected to be separated completely by this method. However, in this study it was found that cerium concentrate started to form only after addition of Na_2CO_3 solution at around pH 3. The analysis content of cerium concentrate was as shown in Table 1 where Ce was the most abundant element followed by Nd, La, and Pr that were co-precipitated. After the filtrate was further added with more Na_2CO_3, cerium was also detected in what was expected to be the other RE concentrate. Ce was the most concentrated element although it was expected that it should be less than that. This suggests that Ce (III) oxidation in this study was not completed. This observation can be caused by the chemical dynamics of the oxidation-hydrolysis reaction and the resulting pH instability. As in Equation (1), the oxidation of Ce^{3+} to Ce^{4+} using permanganate is accompanied by the release of H^+ ion, which rapidly lowers the pH of the solution. For effective separation, cerium must precipitate as $Ce(OH)_4$ which is also highly soluble in highly acidic conditions. Rapid generation of H^+ ion is likely to overwhelm the buffering capacity of the added Na_2CO_3, resulting in drop in pH to below threshold required for stable precipitate formation. This eventually makes it difficult to complete the hydrolysis of Ce^{4+}; therefore, a significant portion of cerium remained in the filtrate. As reported in recent kinetic studies, Ce (IV) species are highly sensitive to re-dissolution in acidic nitrate media compared to chloride systems where complexation stability differs significantly (Abdulvaliyev et al., 2024). Hence, a significant amount of cerium remained in the filtrate. Table 1 displayed the incomplete separation where cerium can still be detected after the process.

Table 1: Elemental composition of Ce and other RE concentrate obtained from the separation of the elements dissolved in nitric acid solution

Element	Concentration in Ce concentrate	concentration in other RE concentrate
Ce	45.5 %	43.9 %
Nd	13.7 %	18.8 %
La	8.4 %	20.3 %
Pr	3.6 %	4.3 %
Mn	18.5 %	(not detected)
Others	9.3 %	12.6 %

$KMnO_4$ is more stable at pH more than 2.5. However, the more $KMnO_4$ added, the pH of the solution will be reduced and eventually will affect the oxidation process. This could be explained by the formation of H^+ ions as described in Equation (1). Therefore, to maintain the pH, Na_2CO_3 needs to be added. The oxidation process of Ce (III) with $KMnO_4$ was described in Equation (2) – (4). It showed that apart from forming Ce (IV) as $Ce(OH)_4$, manganese (IV) oxide will be produced as impurity, hence affecting the purity of cerium. Fortunately, MnO_2 can be removed by dissolving it in dilute HCl.

$$3Ce^{3+} + MnO^{4-} + 10H_2O \leftrightarrow 3Ce(OH)_4\,(s) + MnO_2\,(s) + 8H^+\,(aq) \quad (1)$$
$$3Ce(NO_3)_3 + KMnO_4 + 2H_2O \leftrightarrow 2Ce(NO_3)_4 + Ce(OH)_4 + KNO_3 + MnO_2 \quad (2)$$
$$Ce(NO)_3 + 4H_2O \leftrightarrow Ce(OH)_4 + 4HNO_3 \quad (3)$$
$$HNO_3 + Na_2CO_3 \leftrightarrow NaNO_3 + H_2O + CO_2 \quad (4)$$
$$2MnO^{4-} + 8H^+ + 6Cl^- \leftrightarrow 2MnO_2 + 3Cl_2 + 4H_2O \quad (5)$$

b. HCl as the dissolution medium.

HNO_3 was then substituted with hydrochloric acid. This method was reported by McNeice (2018) & Sauber (2018). $RE(OH)_3$ were dissolved in 2 M and 37 % (v/v) concentration and it was found that 2 M HCl is sufficient to dissolve $RE(OH)_3$. Therefore, it is recommended that highly concentrated HCl should not be used since it can give more risks in terms of environment, health and safety if not handled properly. Besides that, there were dark coloured particles observed in both acidic concentrations, but it will dissolve upon addition of water for dilution.

Unlike before, the pH for this reaction was controlled and kept above pH 2.5. This is because, under low pH, MnO_4^- will react with H^+ and Cl^- ions to form solid MnO_2 (Eq. 5), hence affecting the oxidation process as no MnO_4^- ions will be available to oxidise Ce (III). Meanwhile, $KMnO_4$ was added until the purple colour did not disappear, indicating no more Ce (III) to be oxidized. Table 2 illustrates the percentage concentration of elements found in the products formed from both solutions and Figure 1 illustrated the elements presence in the concentrate as hydroxides. As expected, Ce was not found in the other RE concentrate. This suggested that Ce successfully separated through oxidation process. The concentration of Ce in the Ce concentrated was at around 70% together with 15.2 % Nd, Mn and some REEs. As for the REE concentrate, more Nd detected with concentration of more than 30 % together with La (>20 %), Pr (> 10 %) and other elements.

Table 2: Elemental composition of Ce and other concentrate obtained from dissolving the rare earth hydroxide concentrate in 2M and 37 % HCl.

	2 M HCl acid		37 %(v/v) HCl	
Elements	**(Ce concentrate)**	**(other REE concentrate)**	**(Ce concentrate)**	**(other REE concentrate)**
Ce	71.2 %	(Not detected)	70.6 %	(Not detected)
Nd	15. 2 %	37.6 %	15.2 %	30.9 %
Mn	7.7 %	(Not detected)	7.5 %	(Not detected)
La	(Not detected)	31.1 %	(Not detected)	22.1 %
Pr	(Not detected)	12.6 %	(Not detected)	10.2 %
Cl	4.2 %	11.6 %	3.2 %	26.5 %
Other REEs	0.8 %	6.8 %	1.0 %	9.8 %
Other elements	0.7 %	0.3 %	2.5 %	0.6 %

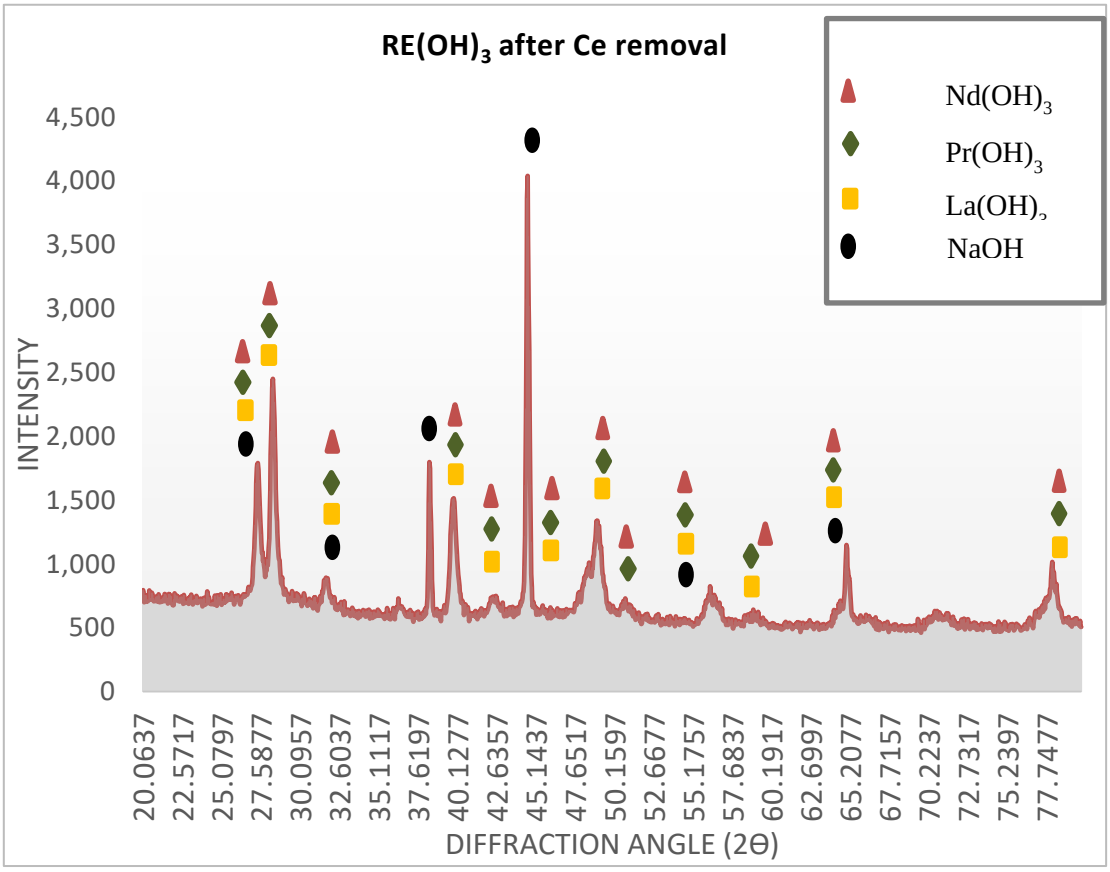

Figure 1: X-ray Diffraction (XRD) analysis on the $RE(OH)_3$ after Ce separation shows no $Ce(OH)_4$ detected indicating cerium was removed completely from the mixed rare earth hydroxide concentrate.

c. Separation of Nd and La.

Separation of Nd and La were obtained by precipitating $Nd(OH)_3$ before $La(OH)_3$. This is due to the difference in the solubility product constants (Ksp) of both hydroxides (Wai, 2018). $Nd(OH)_3$ has a smaller Ksp value than $La(OH)_3$, suggesting that $Nd(OH)_3$ is less soluble in ammonia solution, hence it will precipitate first. ED-XRF analysis of both concentrates in Figure 2 showed that Nd can be fully separated from La at pH 7.5 with 9.9% La present. Meanwhile, Sm prefers to be separated along with Nd while Pr prefers to be with La.

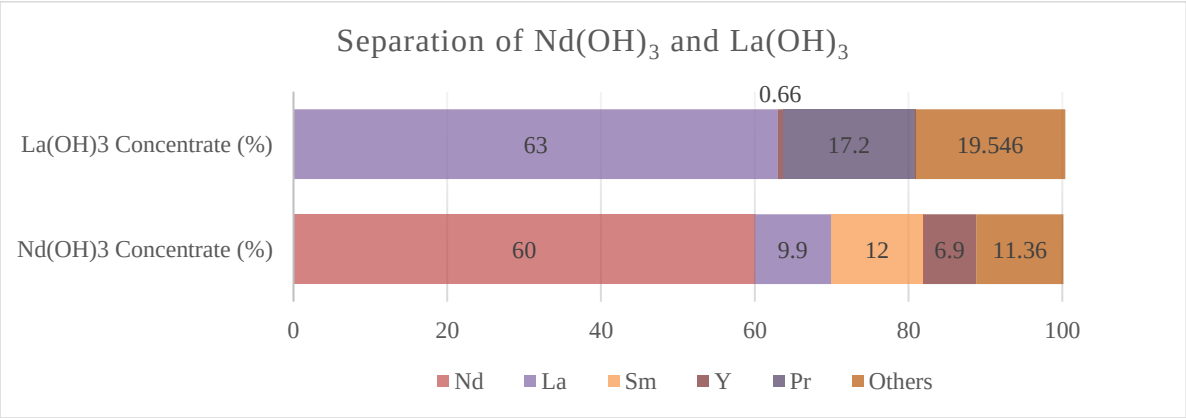

Figure 2: Major elements obtained through analysis result of analysis using ED-XRF for $Nd(OH)_3$ and $La(OH)_3$ concentrate

CONCLUSION

This study compared the effectiveness of HNO_3 and HCl as dissolution media for the oxidative separation of cerium from rare earth hydroxides ($RE(OH)_3$). The investigation revealed that the nitric medium was less effective due to pH instability during the oxidation process, which hindered the complete precipitation of Ce(IV). Further optimization in terms of acid concentration and pH control would be necessary to make the nitrate route viable. Meanwhile, the use of 2 M HCl was proven to be more effective for dissolving $RE(OH)_3$ and facilitating cerium separation. This concentration is sufficient for dissolution while offering safer and greener separation processes for cerium and lanthanum, as emphasized in recent recovery studies (Vargas et al., 2021). Through this method, cerium was successfully separated with approximately 71.2% purity, although small amount of MnO_2 impurities were present. Other than that, the following selective precipitation at pH 7.5 successfully isolated lanthanum from neodymium since neodymium was absent in the lanthanum concentrate. These findings suggest that the 2 M HCl route is a promising method for enhancing the extraction of individual rare earth elements from Malaysia monazite.

ACKNOWLEDGEMENTS

This study is under the PQRD project NM-R&D-23-14 (Removal of Cerium from Malaysian Monazite for Neodymium Solvent Extraction Enhancement).

REFERENCES

Abdulvaliyev, R., Ultarakova, A., Mukangaliyeva, A., Lokhova, N., & Kassymzhanov, K. (2024). Comparative analysis of acid leaching for the efficient recovery of lanthanum and cerium from phosphate. *Separations*, *11*(10), 288. https://doi.org/10.3390/separations11100288

Formiga, T., & Morais, C.A., (2016). Cerium separation from kight rare earth concentrate by liquid-liquid extraction. *World Journal of Engineering and Technology. 4*(1), 129-137.

McNeice, J.A. (2018). An Investigation into cerium oxidation under acidic conditions *[Master's thesis, Queen's University].*

Morais, C.A., Benedetto, J.S., & Ciminelli V.S.T. (2003). Recovery of cerium by oxidation/hydrolysis with KMnO4 – Na_2CO_3, *Electrometallurgy and Environmental Hydrometallurgy*. 2.

Purwani, M.V. & Trinopiawan, K. (2019). Separation of Ce, La, and Nd in rare earth hydroxide (REOH) by oxidation with potassium permanganate and precipitation, *Journal of Physics: Conference Series 1198*, 032003.

Rice, A. C. (1959). *Preparation of rare earth chloride solutions* (Report of Investigations 5499). U.S. Department of the Interior, Bureau of Mines.

Sauber, M.E. (2018). Oxidative removal of cerium from rare earth elements mixed chloride solution. In Davis, B., *et al.* (Eds.) *Extraction 2018*. (The Minerals, Metals & Materials Series. Springer, Cham) Springer.

Suyanti, S., Daulay, A., Astuti, W., Widana, K. S., Petrus, H. T. B. M., & Adi, W. A. (2025). Separation of cerium from rare earth elements hydroxide using dilute nitric acid and potassium permanganate. *Canadian Metallurgical Quarterly*. Advance online publication. https://doi.org/10.1080/00084433.2025.2609470

Vapnik, H., Kim, H.E., Kim, Y., Ooi, A.W.S., Vibbert. H. B., Park, A.H.A., Su, X. (2025). Selective electrochemical recovery of cerium over lanthanum from complex waste feedstocks by alternating current electro-precipitation, *Chemical Engineering Journal*, *504*, 158537. https://doi.org/10.1016/j.cej.2024.158537

Vargas, C., Crampon, M., Cognet, P., & Fermen-Coker, M. (2021). Green separation of lanthanum, cerium and nickel from waste nickel metal hydride battery leachate using aqueous biphasic systems. *Waste Management*, *125*, 154-162.

Wai, A.M. (2018) . Selective precipitation of neodymium oxide (Nd_2O_3) from monazite, *International Journal of Science, Engineering and Technology Research (IJSER) 8*(8)

Jurnal Sains Nuklear Malaysia, 2026, 38(Special Issue): 25 – 36
ISSN: 2232-0946

FABRICATION OF POLYVINYLIDENE FLUORIDE-BASED POLYMER INCLUSION MEMBRANES FOR THE SELECTIVE EXTRACTION OF RARE EARTH ELEMENTS FROM ELECTRONIC WASTE LEACHATES

Fathiyyah Nadhirah Abdul Fauzi[1], Maziati Akmal M.H.[2*], Wan Syasya Nabilah[3], Wafiuddin Ismail[1] and Ahmad F.B.[3]

[1] Department of Chemistry, Kulliyyah of Science,
International Islamic University Malaysia (IIUM),
25200, Kuantan, Pahang, Malaysia
[2]Department of Science in Engineering, Kulliyyah of Engineering,
International Islamic University Malaysia (IIUM), Jalan Gombak,
53100 Kuala Lumpur, Malaysia
[3]Department of Chemical Engineering & Sustainability, Kulliyyah of Engineering,
International Islamic University Malaysia (IIUM), Jalan Gombak,
53100 Kuala Lumpur, Malaysia
[*]Correspondence author: maziatiakmal@iium.edu.my

ABSTRACT

Rare earth elements (REEs) are important materials of modern technologies, but these elements are difficult to obtain from conventional mining due to both environmental and geopolitical reasons, which has led to the exploration of secondary sources such as e-waste. Herein, we report on the early-stage development and evaluation of PIMs, prepared using PVDF, with the aim of extracting REEs. Membranes were fabricated using three different solvents, namely dimethylacetamide (DMAc), N-methyl-2-pyrrolidone (NMP), and dimethylformamide (DMF), using the NIPS technique and then quenched with either water or air. The membranes were characterized by analyzing the mechanical strength, thickness, and morphology, and the results were analyzed to determine the influence of fabrication conditions on the structural properties relevant to REE transport. The results indicated that water-quenched membranes were generally thicker than air-quenched ones, whereas membranes made with NMP had the highest tensile strength, at approximately 4.3 MPa. Scanning Electron Microscopy (SEM) images of the membranes confirmed that those fabricated with DMAc had the most porous structure, followed by DMF and NMP, which is consistent with the lower swelling index (40.68%) and higher water absorption (8.94%) of these membranes, allowing extractants to diffuse more readily through the membrane. Overall, these results demonstrate that the choice of solvent and quenching method is critical to the determination of the membrane strength and porosity, two properties that are critical to the efficient extraction of REEs, and future work will incorporate ionic liquid extractants and assess the transport of REEs from e-waste leachates.

Keywords: Rare Earth Elements; Polymer Inclusion Membranes; Electronic waste; Polyvinylidene Fluoride; Nonsolvent Induced Phase Separation

INTRODUCTION

Rare earth elements (REEs) form a collection of 17 chemically similar elements that can be found in the central region of the periodic table (atomic numbers 21, 39, and 57–71) (Bashiri et al., 2022). They are critical in both traditional and emerging industries, with applications ranging from consumer electronics and renewable energy to lighting and medical technology (Ali et al., 2022a; Balaram, 2019; Liu et al., 2019). These elements are essential in a variety of technologies, including fluorescent lights, lasers, superconducting magnets, atomic power sources, and turbine engines (Dev et al., 2020; Golroudbary et al., 2022; Haque et al., 2014). Interestingly, while they are called "rare," these elements are not rare at all, as they appear in the Earth's crust in higher abundance than precious metals like gold or platinum (Croft et al., 2024). The challenge is extracting them, which is technologically problematic and costly because REEs appear in small quantities, usually in parts per billion (ppb). Their principal mineral sources include monazite, xenotime, lanthanide, allanite, bastnäsite, loparite, and phosphate minerals (Ali et al., 2022).

Ironically, despite the fact that REEs are critical for modern and green technologies, the industrial extraction of REEs from ores often leads to high environmental contamination and production costs (Hammache et al., 2021; Liang et al., 2024). Furthermore, the separation of REEs is extremely difficult because of the similarity on chemical and physical properties, which has made it necessary to develop sustainable and environmentally friendly methods for recovery (Filho et al., 2023). Numerous techniques such as solvent extraction, ion exchange, precipitation, crystallization, and adsorption have been explored over the years to recover REEs from various sources, including mineral ores, industrial byproducts, and even environmental samples (Pavón et al., 2022; Quijada-Maldonado & Romero, 2021; W. Zhang et al., 2020). Although these techniques have been useful for selective separation, they have limitations, including low selectivity and purity of the recovered elements, the large amount of waste generated, and the large number of chemical reagents used (Chen & Zheng, 2019). Taken together, these challenges emphasize the need for greener and more efficient strategies for REE recovery.

In place of conventional solvent extraction techniques, polymer inclusion membranes, or PIMs, have shown great promise. The components of these membranes are a plasticizer, a carrier (extractant), and a base polymer (Croft et al. in 2018). Among these materials, PVDF-based PIMs stand out as promising choices. The homopolymerization or copolymerization of vinylidene fluoride monomers produces PVDF, which is known for its exceptional flexibility, wear resistance, and resistance to impacts and environmental contaminants (Kazemi and Yaftian, 2024; Turgut et al. 2017; Zheng and colleagues, 2018). Polymer inclusion membranes (PIMs) are more stable than many traditional liquid-liquid extraction systems, but they are still not durable enough to be used on a large scale in industry (Kazemi & Yaftian, 2024; Kogelnig et al., 2011). As a result, recent research has increasingly focused not only on improving membrane stability but also on optimizing other critical performance factors, such as extraction rates and extractive capacity.

In this study, the properties of PVDF-based PIMs fabricated by the phase inversion technique were examined in relation to the combined effects of solvent type, quenching method, and PVDF concentration. Additionally, this work addresses difficulties in membrane fabrication by analyzing significant mechanical, structural, and physical parameters. Physical characterization involves tensile strength tests as well as the analysis of morphology, swelling index, and water uptake. On the other hand, chemical characterization focuses on identifying functional groups using Fourier Transform Infrared Spectroscopy (FTIR).

MATERIALS AND METHODS

Materials

Polyvinylidene fluoride (PVDF) with an average molecular weight of 180,000 g/mol was obtained from Sigma-Aldrich and used as the base polymer in this study. Aliquat 336 ($C_{25}H_{54}ClN$). Additionally, a quaternary ammonium salt with a molecular weight of 404.16 g/mol, was also sourced from Sigma-Aldrich and employed as an extractant. As solvents, N, N-dimethylformamide (DMF, C_3H_7NO; 73.09 g/mol), N,N-dimethylacetamide (DMAc, C_4H_9NO; 87.12 g/mol), and dimethyl sulfoxide (DMSO, $(CH_3)_2SO$; 78.13 g/mol) were all purchased from Sigma-Aldrich. Deionized water with a resistivity of 18 MΩ·cm, produced in-house using a laboratory-grade purification system, was used for all experimental procedures.

Fabrication of PVDF-based PIM via Phase Inversion

The membranes were fabricated using the non-solvent induced phase separation (NIPS) method, with PVDF as the base polymer. To evaluate the influence of processing conditions, formulations were prepared with different solvents (DMAc, NMP, and DMF) and at varying PVDF concentrations. For each formulation, 3.00 g of PVDF pellets were dissolved in 30 mL of solvent, maintaining a ratio of 1 mL of solvent per 0.1 g of polymer (Hoque et al., 2019). The solutions were stirred at 60 °C for approximately 2 hours until complete dissolution was achieved, then cast evenly onto a glass plate supported with non-woven fabric.

Two quenching methods were applied. In the water quenching process, the cast film was immediately immersed in a precipitation bath at room temperature. In the air quenching method, the film was briefly exposed to ambient air before immersion. After quenching, the membranes were dried for 24 hours and subsequently cut to appropriate sizes for further analysis.

Characterization of PVDF-based PIM

A combination of four analytical techniques was employed to evaluate the physical, chemical, structural, and mechanical properties of the fabricated membranes.

Functional group analysis

Fourier Transform Infrared Spectroscopy (FTIR) was used to identify functional groups present in the membranes. Spectra were collected in the range of 4000–400 cm^{-1} with a resolution of 4 cm^{-1}, using transmittance mode and 32 scans at room temperature.

Morphological analysis

The surface morphology of the membranes was examined using Scanning Electron Microscopy (SEM). Prior to imaging, the pre-dried PVDF membranes were coated with platinum. Observations were carried out at a magnification of 3000×.

Mechanical properties analysis of the PVDF-PIMs

The tensile strength of the PVDF-PIMs was measured following the procedure described by Baczyńska et al. (2018). Tests were conducted at room temperature using a universal testing machine (SHIMADZU), as shown in Figure 1. Membrane samples were cut into strips measuring 5 cm in length and 0.5 cm in width, and each strip was clamped vertically between two pairs of 50 mm forceps. To ensure reliability, three replicates were tested for each sample, and the average value was reported.

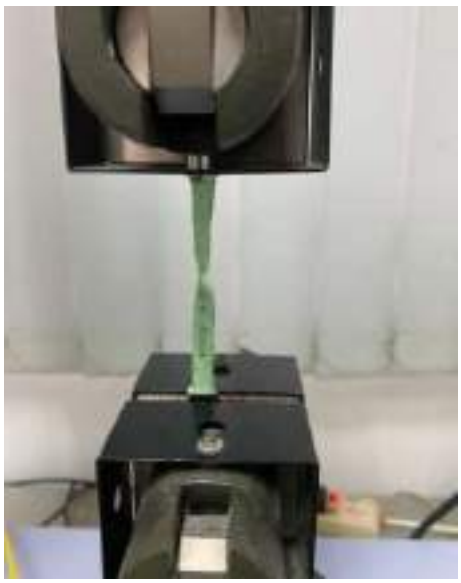

Figure 1: Tensile strength test using Universal Tensile Machine (UTM)

Physical properties analysis of the PVDF-PIMs

Water uptake (WU, %) and swelling degree (SD, %) were determined to assess the physical characteristics of the membranes. Dried PVDF-PIMs were cut into strips of approximately 30 × 10 mm and immersed in deionized water at 25 °C for 48 hours. After immersion, the samples were gently blotted with absorbent paper to remove surface water. Water uptake was then calculated using Equation (1):

$$WU = \frac{(m_{hydrated} - m_{dry})}{(m_{dry})} \times 100\% \quad (1)$$

where m_{dry} is the membrane mass before immersion and $m_{hydrated}$ is the membrane mass after immersion.

The swelling degree was measured by comparing membrane thickness before and after immersion, as shown in Equation (2):

$$SD = \frac{(x_{hydrated} - x_{dry})}{(x_{dry})} \times 100\% \quad (2)$$

where x_{dry} represents the thickness of the dry membrane and $x_{hydrated}$ is the thickness after immersion.

RESULTS AND DISCUSSION

Swelling index and water uptake measurement

The swelling index indicates how much a membrane swells when absorbing a liquid, often water. The membrane's thickness or volume changes because of this absorption. Water uptake, however, indicates the total amount of water absorbed by the membrane without showing any physical expansion (Zheng et al., 2018).

According to Table 1, the membrane fabricated using DMAc and subjected to air quenching exhibits the lowest swelling index (40.68%) and the highest water uptake (18.94%) compared to those

prepared with NMP and DMF. During absorption, hydrogen bonds form between water molecules and the active sites of the carrier. More carrier content means more active sites, allowing for greater water retention in the membrane (Elozeiri et al., 2024). These findings suggest that DMAc is a preferable solvent for producing highly porous membranes for REE extraction.

Table 1: Swelling index and water uptake results

Type of Quenching	Solvent	Water Uptake (%)	Swelling Index (%)
Air	DMAc	18.94	40.68
	NMP	9.28	79.63
	DMF	11.32	61.54
Water	DMAc	18.75	42.11
	NMP	13.69	78.85
	DMF	13.34	81.84

Thickness of PVDF-PIMs measurement

PVDF-PIMs prepared with DMAc and DMF became noticeably thicker after immersion in water compared to those exposed to air (Figure 2). This is most likely caused by pore enlargement from water absorption when soaking. Additionally, solvents that attract water, like DMAc and DMF, often cause the polymer to precipitate quickly. Rapid precipitation can cause pore expansion and an increase in membrane thickness (Bashiri et al., 2022). Quenching in water accelerates phase separation, resulting in membranes with more porosity and a higher tendency to expand while absorbing water. The observed changes in membrane thickness after immersion reflect the degree of swelling, which is closely associated with the membrane's internal structure, particularly its porosity and hydrophilic character (Venault et al., 2014).

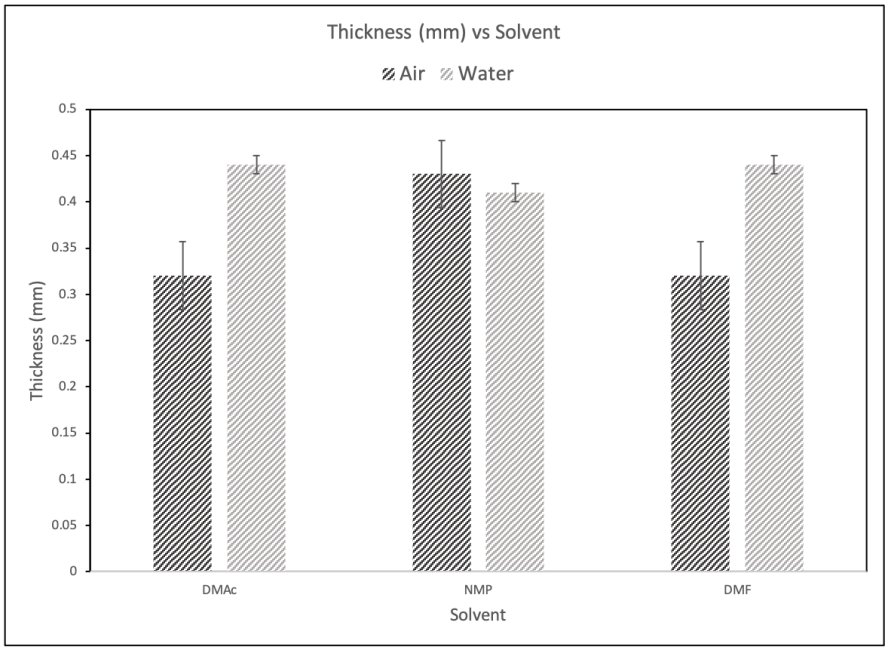

Figure 2: Thickness of PVDF-PIMs dissolved in different solvents

Tensile strength analysis

The tensile strength results obtained from the Universal Tensile Machine (UTM) for membranes prepared under different solvent systems and quenching conditions are presented in Figure 3. Of the samples tested, the membrane made with DMAc as the solvent and air quenched has a moderate tensile strength of 4.07 MPa. Typically, mechanical strength values between 2 and 4 MPa are considered sufficient for REE extraction, where membranes work under low-pressure conditions for long periods. Applying higher pressure may compress the polymer structure, which in turn could interfere with the membrane's ability to maintain stable REE transport performance (Anim-Mensah et al., 2025).

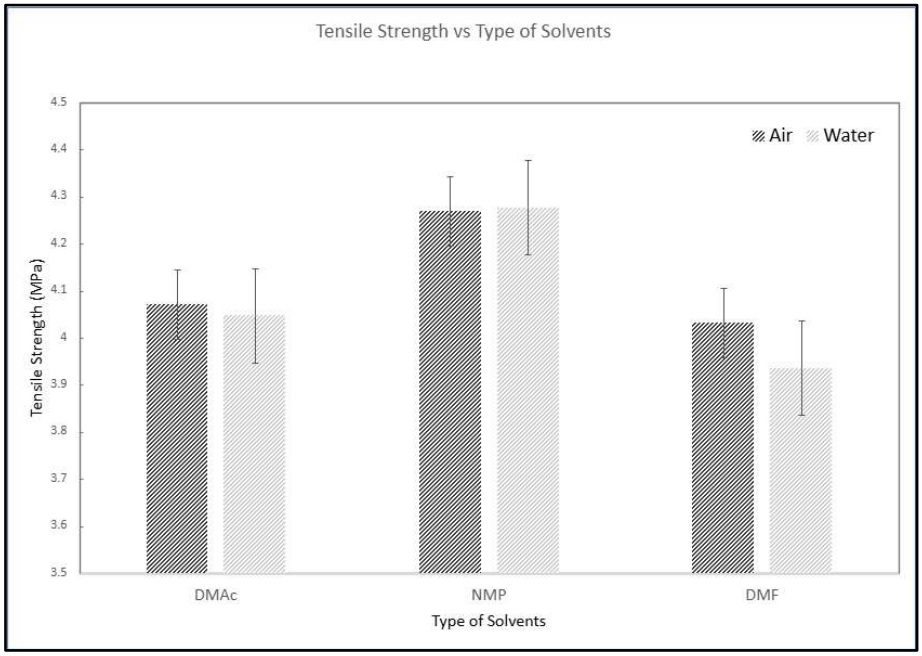

Figure 3: Tensile strength of PVDF-PIMs dissolved in varying solvents and quenching conditions

Morphology analysis

The SEM micrographs displayed in Figure 4 demonstrate the cross-sectional structure of PVDF-based PIMs created with various solvents at a 3000× magnification. The choice of solvent affects the membrane's structure due to differences in properties, like volatility, viscosity, and compatibility with the nonsolvent. The membrane made with DMAc shows a highly porous structure with many interconnected macrovoids, indicating fast phase inversion due to quick solvent-nonsolvent exchange. This observation matches the findings of AlMarzooqi et al. (2016), who concluded that membranes made solely with DMAc solvent develop a two-part structure consisting of finger-like and sponge-like sections.

As seen in Figure 5, the membrane fabricated with a PVDF concentration of 1.0 g/L exhibits a highly porous and interconnected structure, marked by large, round, and evenly distributed voids. This clear morphology is more defined than membranes made with 0.5 g/L and 0.75 g/L PVDF. Fundamentally, the interconnected pore network in the membrane prepared at a concentration of 1.0 g/L facilitates the movement and transport of REE ions, thereby enhancing both permeability and selectivity. This

enhancement is due to the direct and efficient pathways it provides for REE ion migration through the mesoporous surface layer and the macrovoids-rich bulk layer (Cheng & Bae, 2024).

In comparison, the membrane containing 0.5 g/L PVDF exhibits a very open yet uneven pore morphology, characterized by thin polymer walls and macrovoids. Hence, the overall network from 0.5 g/L PVDF concentration appears disordered and less structured.

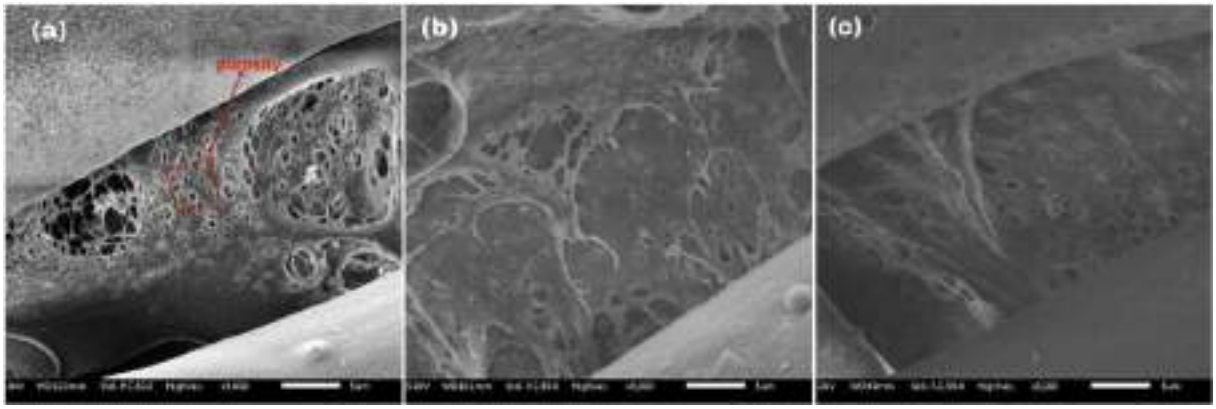

Figure 4: SEM results of PVDF-PIMs dissolved in different solvents (a) DMAc, (b) DMF, (c) NMP at 3000 times magnification

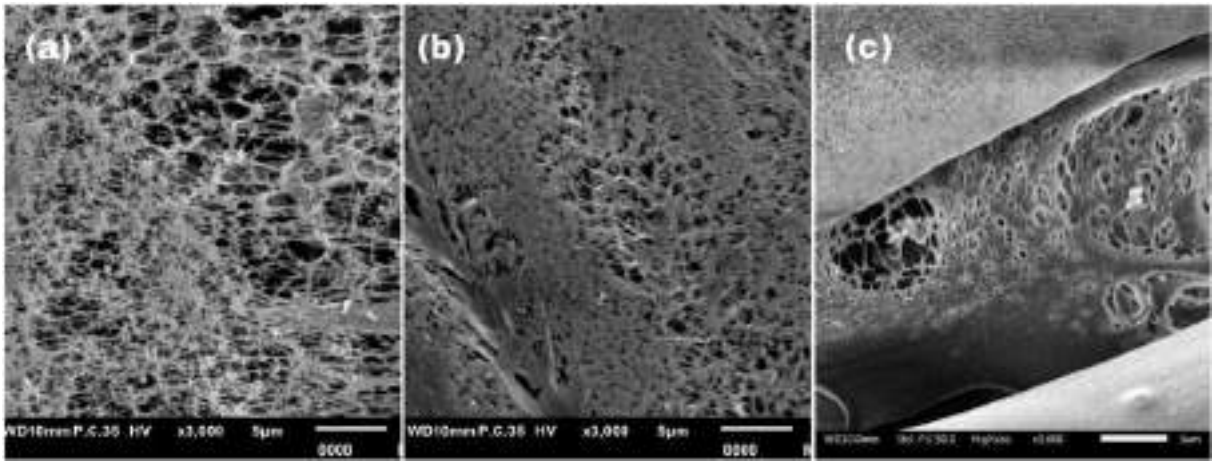

Figure 5: SEM results of PVDF-PIMs dissolved in different PVDF concentrations using DMAc solvent (a) 0.5 g/L, (b) 0.75 g/L, (c) 1.0 g/L at 3000 times magnification.

Functional group analysis

FTIR spectroscopy was used to analyze the chemical structure and phase composition of PVDF membranes produced with 3 different types of solvents (DMAc, DMF, NMP) and varied PVDF concentrations (0.5, 0.75, and 1.0 g/mL). Figure 6 illustrates the comparison of FTIR spectra for PVDF membranes cast with varied solvents. The characteristic peaks of the β-phase of PVDF were observed at 841 and 1240 cm^{-1}, which are linked to CF_2 stretching and skeletal vibrations characteristic of the polar crystalline arrangement (Li et al., 2013). All membranes exhibited characteristic absorption bands of PVDF, which are peaks at 840 cm^{-1} (CF_2 stretching), 872 and 720 cm^{-1} (CH_2 rocking), 1240 cm^{-1} (CF_2 asymmetric stretching), 1406 cm^{-1} (CH_2 bending), and the region between 1016 and 1092 cm^{-1} (C–F stretching) (Barrau et al., 2018).

Several of these peaks, specifically at 490, 720, 872, 1016, and 1406 cm^{-1} are linked to the α-phase of PVDF which correspond to CF_2 wagging, CH_2 rocking, and CF_2 wagging, and non-polar backbone

vibrations. In addition, the presence of a C=O peak around 1710 cm^{-1} indicates residual solvent traces, most likely from DMAc, DMF, or NMP (Cai et al., 2017).

Figure 7 shows the comparison when using different PVDF concentrations. The FTIR spectra indicated that as the concentration of PVDF increased, the baseline noise decreased, suggesting enhanced membrane uniformity and stronger polymer matrix formation. While all concentrations displayed both α- and β-phase signals, the α-phase peaks became increasingly dominant at higher PVDF content, especially at 1.0 g/mL.

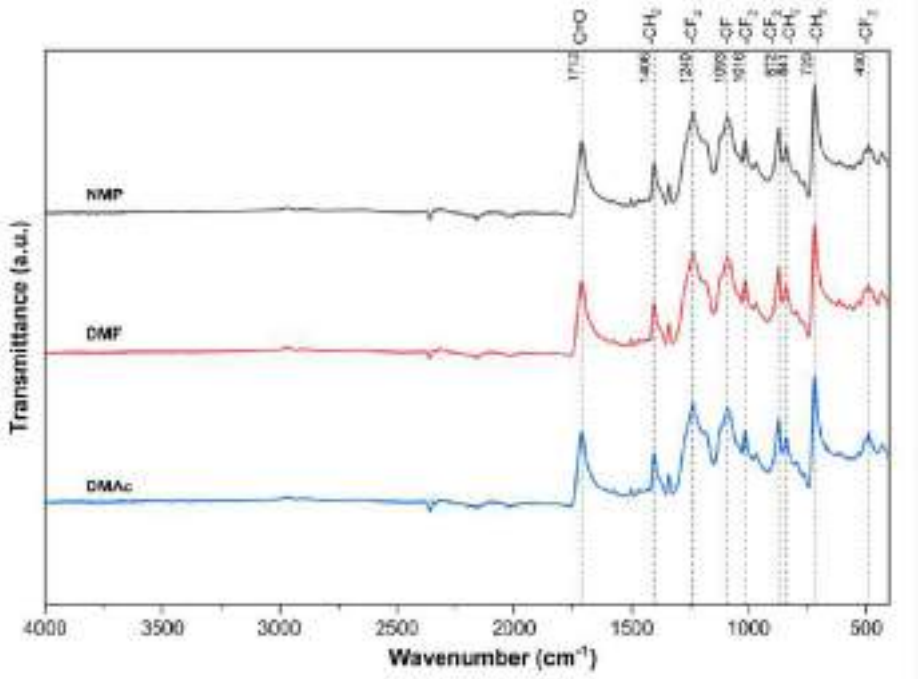

Figure 6: FTIR Spectra of PVDF-PIMs dissolved in different solvents (NMP, DMF, DMAc)

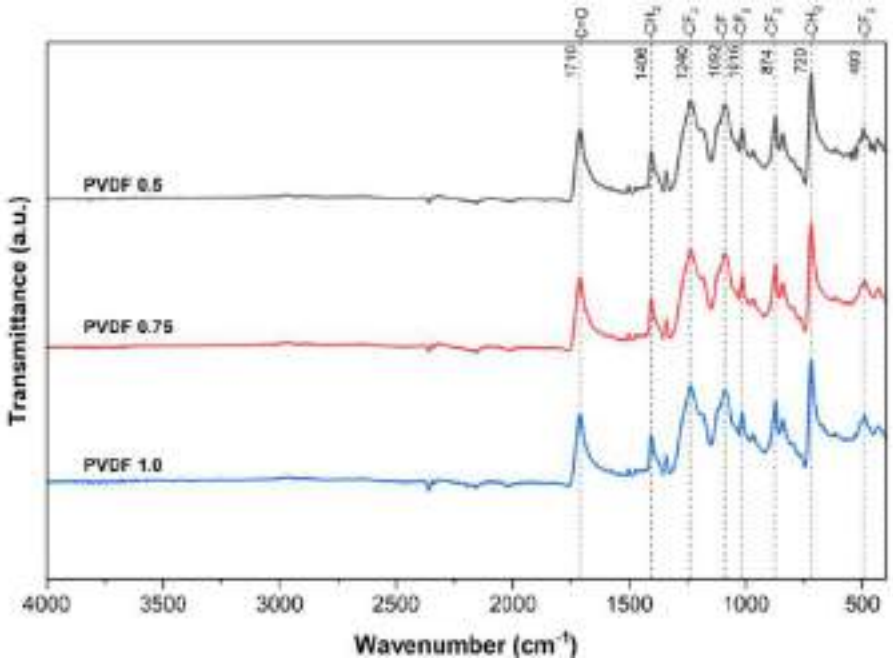

Figure 7: FTIR Spectra of PVDF-PIMs with different PVDF concentrations (0.5, 0.75, 1.0 g/L)

CONCLUSION

In conclusion, the comprehensive evaluation of the synthesized PVDF-PIM membranes has elucidated the critical parameters influencing membrane efficiency in REE extraction. This study effectively identified that the optimal combination of solvent and quenching method is DMAc with air quenching, which resulted in a remarkable swelling index of 40.68% and the highest water uptake at 18.94%. The membranes demonstrated moderate tensile strength of 4.07 MPa and a highly porous network, characterized by interconnected macrovoids that significantly enhance their performance.

A detailed examination of the PVDF concentration revealed that membranes fabricated with 1.0 g/L PVDF exhibited the best overall properties, balancing higher water uptake (4.71%) with relatively low swelling index (6.67%), suggesting a balance between hydrophilicity and dimensional stability, and developing a more defined porous structure, which is closely related to improved permeability and mechanical strength. Functional group characterization further validated these results by indicating the molecular organization of the 1.0 g/L membrane, which can be correlated with its chemical stability and suitability for long-term performance in separation applications.

To advance the applicability of PVDF-PIMs in more challenging environments, future research should expand the range of characterization tests carried out. For instance, water contact angle measurements would be useful to better understand how the membrane surface interacts with liquids, which in turn affects wetting behavior and ion transfer efficiency. In addition, studying how variations in water bath temperature during the quenching process influence pore development and membrane morphology could reveal important insights. These assessments would allow a clearer link to be established between fabrication conditions, surface properties, and overall membrane stability, providing a stronger basis for tailoring membranes to specific applications.

In addition to surface and quenching analyses, another critical direction for future work is to examine how physical structure and mechanical performance influence membrane functionality. Furthermore, the correlation among membrane thickness, ion transport rates, and tensile strength will be essential for maximizing the extraction efficiency of rare earth elements. A thicker membrane may offer mechanical durability but may slow ion transfer, whereas thinner membranes may offer higher transport rates at the cost of strength. A systematic study of these trade-offs is necessary. The structural and chemical characteristics of PVDF-PIMs can be carefully tuned to optimize performance for laboratory testing as well as for long-term industrial operation where durability, selectivity, and consistent performance are all necessary.

ACKNOWLEDGEMENTS

The work in this manuscript was funded by the Ministry of Higher Education Malaysia (FRGS/1/2024/TK09/UIAM/02/1).

REFERENCES

Ali, A. H., Dakroury, G. A., Hagag, M. S., Abdo, S. M., & Allan, K. F. (2022a). Sorption of Some Rare Earth Elements from Acidic Solution onto Poly(acrylic acid–co-acrylamide/16, 16-dimethylheptadecan-1-amine) Composite. Journal of Polymers and the Environment, 30(3), 1170–1188. https://doi.org/10.1007/S10924-021-02271-7/FIGURES/2

AlMarzooqi, F. A., Bilad, M. R., Mansoor, B., & Arafat, H. A. (2016). A comparative study of image analysis and porometry techniques for characterization of porous membranes. Journal of Materials Science, 51(4), 2017–2032. https://doi.org/10.1007/s10853-015-9512-0

Anim-Mensah, A. R., Drouiche, N., Farrukh, S., & Alshami, A. (2025). Pressure-driven polymeric membrane performance prediction, new membrane dimensionless number, and considerations for effective membrane design, selection, testing, and operation. Frontiers in Membrane Science and Technology, 3, 1454589. https://doi.org/10.3389/FRMST.2024.1454589

Baczyńska, M., Waszak, M., Nowicki, M., Przadka, D., Borysiak, S., & Regel-Rosocka, M. (2018). Characterization of Polymer Inclusion Membranes (PIMs) Containing Phosphonium Ionic Liquids as Zn(II) Carriers. Industrial and Engineering Chemistry Research, 57(14), 5070–5082. https://doi.org/10.1021/acs.iecr.7b04685

Balaram, V. (2019). Rare earth elements: A review of applications, occurrence, exploration, analysis, recycling, and environmental impact. Geoscience Frontiers, 10(4), 1285–1303. https://doi.org/10.1016/J.GSF.2018.12.005

Barrau, S., Ferri, A., Da Costa, A., Defebvin, J., Leroy, S., Desfeux, R., & Lefebvre, J. M. (2018). Nanoscale Investigations of α- And γ-Crystal Phases in PVDF-Based Nanocomposites. ACS Applied Materials and Interfaces, 10(15), 13092–13099. https://doi.org/10.1021/ACSAMI.8B02172/SUPPL_FILE/AM8B02172_SI_001.PDF

Bashiri, A., Nikzad, A., Maleki, R., Asadnia, M., & Razmjou, A. (2022). Rare Earth Elements Recovery Using Selective Membranes via Extraction and Rejection. Membranes, 12(1). https://doi.org/10.3390/membranes12010080

Cai, X., Lei, T., Sun, D., & Lin, L. (2017). A critical analysis of the α, β and γ phases in poly(vinylidene fluoride) using FTIR. RSC Advances, 7(25), 15382–15389. https://doi.org/10.1039/C7RA01267E

Chen, Y., & Zheng, B. (2019). What Happens after the Rare Earth Crisis: A Systematic Literature Review. Sustainability 2019, Vol. 11, Page 1288, 11(5), 1288. https://doi.org/10.3390/SU11051288

Cheng, X., & Bae, J. (2024). Recent Advancements in Fabrication, Separation, and Purification of Hierarchically Porous Polymer Membranes and Their Applications in Next-Generation Electrochemical Energy Storage Devices. Polymers 2024, Vol. 16, Page 3269, 16(23), 3269. https://doi.org/10.3390/POLYM16233269

Croft, C. F., Almeida, M. I. G. S., Cattrall, R. W., & Kolev, S. D. (2018). Separation of lanthanum(III), gadolinium(III) and ytterbium(III) from sulfuric acid solutions by using a polymer inclusion membrane. Journal of Membrane Science, 545, 259–265. https://doi.org/10.1016/j.memsci.2017.09.085

Croft, C. F., Nagul, E. A., Almeida, M. I. G. S., & Kolev, S. D. (2024). Polymer-Based Extracting Materials in the Green Recycling of Rare Earth Elements: A Review. ACS Omega, 9(39), 40315–40328. https://doi.org/10.1021/acsomega.4c06990

Dev, S., Sachan, A., Dehghani, F., Ghosh, T., Briggs, B. R., & Aggarwal, S. (2020). Mechanisms of biological recovery of rare-earth elements from industrial and electronic wastes: A review. Chemical Engineering Journal, 397, 124596. https://doi.org/10.1016/J.CEJ.2020.124596

Elozeiri, A. A. E., Lammertink, R. G. H., Rijnaarts, H. H. M., & Dykstra, J. E. (2024). Water content of ion-exchange membranes: Measurement technique and influence on the ion mobility. Journal of Membrane Science, 698, 122538. https://doi.org/10.1016/j.memsci.2024.122538

Filho, W. L., Kotter, R., Özuyar, P. G., Abubakar, I. R., Eustachio, J. H. P. P., & Matandirotya, N. R. (2023). Understanding Rare Earth Elements as Critical Raw Materials. Sustainability (Switzerland), 15(3). https://doi.org/10.3390/su15031919

Golroudbary, S. R., Makarava, I., Kraslawski, A., & Repo, E. (2022). Global environmental cost of using rare earth elements in green energy technologies. Science of The Total Environment, 832, 155022. https://doi.org/10.1016/J.SCITOTENV.2022.155022

Hammache, Z., Bensaadi, S., Berbar, Y., Audebrand, N., Szymczyk, A., & Amara, M. (2021). Recovery of rare earth elements from electronic waste by diffusion dialysis. Separation and Purification Technology, 254, 117641. https://doi.org/10.1016/J.SEPPUR.2020.117641

Haque, N., Hughes, A., Lim, S., & Vernon, C. (2014). Rare Earth Elements: Overview of Mining, Mineralogy, Uses, Sustainability and Environmental Impact. Resources 2014, Vol. 3, Pages 614-635, 3(4), 614–635. https://doi.org/10.3390/RESOURCES3040614

Hoque, B., Almeida, M. I. G. S., Cattrall, R. W., Gopakumar, T. G., & Kolev, S. D. (2019). Effect of cross-linking on the performance of polymer inclusion membranes (PIMs) for the extraction, transport and separation of Zn(II). Journal of Membrane Science, 589. https://doi.org/10.1016/j.memsci.2019.117256

Kazemi, D., & Yaftian, M. R. (2024). PVDF-HFP-based polymer inclusion membrane functionalized with D2EHPA for the selective extraction of bismuth (III) from sulfate media. Scientific Reports, 14(1). https://doi.org/10.1038/s41598-024-62401-8

Kogelnig, D., Regelsberger, A., Stojanovic, A., Jirsa, F., Krachler, R., & Keppler, B. K. (2011). A polymer inclusion membrane based on the ionic liquid trihexyl(tetradecyl) phosphonium chloride and PVC for solid-liquid extraction of Zn(II) from hydrochloric acid solution. Monatshefte Fur Chemie, 142(8), 769–772. https://doi.org/10.1007/S00706-011-0530-6/FIGURES/2

Li, L., Zhang, M., Rong, M., & Ruan, W. (2013). Studies on the transformation process of PVDF from α to β phase by stretching. RSC Advances, 4(8), 3938–3943. https://doi.org/10.1039/C3RA45134H

Liang, B., Gu, J., Zeng, X., Yuan, W., Rao, M., Xiao, B., & Hu, H. (2024). A Review of the Occurrence and Recovery of Rare Earth Elements from Electronic Waste. Molecules 2024, Vol. 29, Page 4624, 29(19), 4624. https://doi.org/10.3390/MOLECULES29194624

Liu, B., Zhu, N., Li, Y., Wu, P., Dang, Z., & Ke, Y. (2019). Efficient recovery of rare earth elements from discarded NdFeB magnets. Process Safety and Environmental Protection, 124, 317–325. https://doi.org/10.1016/J.PSEP.2019.01.026

Pavón, S., Haneklaus, N., Meerbach, K., & Bertau, M. (2022). Iron(III) removal and rare earth element recovery from a synthetic wet phosphoric acid solution using solvent extraction. Minerals Engineering, 182, 107569. https://doi.org/10.1016/J.MINENG.2022.107569

Quijada-Maldonado, E., & Romero, J. (2021). Solvent extraction of rare-earth elements with ionic liquids: Toward a selective and sustainable extraction of these valuable elements. Current Opinion in Green and Sustainable Chemistry, 27, 100428. https://doi.org/10.1016/J.COGSC.2020.100428

Turgut, H. I., Eyupoglu, V., Kumbasar, R. A., & Sisman, I. (2017). Alkyl chain length dependent Cr(VI) transport by polymer inclusion membrane using room temperature ionic liquids as carrier and PVDF-co-HFP as polymer matrix. Separation and Purification Technology, 175, 406–417. https://doi.org/10.1016/J.SEPPUR.2016.11.056

Venault, A., Chang, Y., Wu, J. R., & Wang, D. M. (2014). Influence of solvent composition and non-solvent activity on the crystalline morphology of PVDF membranes prepared by VIPS process and on their arising mechanical properties. Journal of the Taiwan Institute of Chemical Engineers, 45(3), 1087–1097. https://doi.org/10.1016/J.JTICE.2013.08.014

Zhang, H. ;, Gao, Y., Zhang, H., & Gao, Y. (2023). Polymeric Materials for Rare Earth Elements Recovery. Gels 2023, Vol. 9, Page 775, 9(10), 775. https://doi.org/10.3390/GELS9100775

Zhang, W., Noble, A., Yang, X., & Honaker, R. (2020). A Comprehensive Review of Rare Earth Elements Recovery from Coal-Related Materials. Minerals 2020, Vol. 10, Page 451, 10(5), 451. https://doi.org/10.3390/MIN10050451

Zheng, L., Wang, J., Yu, D., Zhang, Y., & Wei, Y. (2018). Preparation of PVDF-CTFE hydrophobic membrane by non-solvent induced phase inversion: Relation between polymorphism and phase inversion. Journal of Membrane Science, 550, 480–491. https://doi.org/10.1016/j.memsci.2018.01.013

Jurnal Sains Nuklear Malaysia, 2026, 38(Special Issue): 37 – 42
ISSN: 2232-0946

ENHANCED CERIUM RECOVERY FROM ACIDIC CHLORIDE VIA SYNERGISTIC EXTRACTION

Nurliana Roslan

Material Technology Group, Industrial Technology Division, Malaysian Nuclear Agency, Bangi, 43000 Kajang, Selangor, Malaysia.
Correspondence author: nurliana_r@nm.gov.my

ABSTRACT

The increasing demand for light rare earth elements (LREEs), particularly cerium (Ce), has intensified the need for efficient and environmentally sustainable extraction methods. Conventional solvent extraction systems using single extractants often suffer from limited efficiency and raise environmental concerns due to the use of volatile organic compounds (VOCs). Therefore, improving extraction performance while minimizing environmental impact remains a significant challenge. This study aims to evaluate the effectiveness of synergistic extractant systems in enhancing the extraction efficiency of cerium from an acidic chloride medium. The extraction of Ce from an acidic chloride solution was carried out using binary combinations of trihexyl(tetradecyl)phosphonium bis(2,4,4-trimethylpentyl)phosphinate (Cyphos IL), di-(2-ethylhexyl) phosphoric acid (D2EHPA), tributyl phosphate (TBP), and trioctylmethylammonium chloride (Aliquat 336), all dissolved in kerosene. Equal volumes of the organic and aqueous phases were mixed at room temperature to assess Ce extraction efficiency. Results showed that all synergistic systems substantially improved Ce extraction over single extractants. The D2EHPA/Cyphos IL system exhibited the highest enhancement in extraction efficiency, achieving a 94.1% improvement, followed by TBP/D2EHPA (70.7%), TBP/Cyphos IL (66.2%), D2EHPA/Aliquat 336 (51.6%), Aliquat 336/Cyphos IL (51.2%), and TBP/Aliquat 336 (42.0%). The superior performance of the D2EHPA/Cyphos IL system can be attributed to strong synergistic interactions between the ionic liquid and acidic extractant, which enhance metal complexation and transfer into the organic phase. In conclusion, synergistic extractant mixtures provide a highly effective and potentially greener approach for cerium recovery under ambient conditions, offering improved efficiency over conventional single-extractant systems while addressing environmental concerns associated with VOC emissions.

Keywords: Rare earth elements, cerium, synergistic, single extractant, efficiency

INTRODUCTION

Rare earth elements (REEs) are critical materials in modern technologies due to their unique magnetic, catalytic, and electronic properties, with demand continuing to rise as a result of their extensive use in a wide range of high-tech applications (Hamzat et al., 2025; Balaram, 2019). Among them, cerium (Ce), a light rare earth element (LREE), is one of the most abundant and widely used, particularly in catalytic converters, glass polishing, and fuel additives. Its high industrial demand, coupled with its relatively large proportion in REE ores such as monazite, makes cerium an important target for recovery and separation processes (Allahkarami & Rezai, 2021). Despite its abundance, the selective recovery of cerium remains challenging due to the similar chemical properties shared among REEs. Efficient separation is especially critical when cerium coexists with other LREEs in mixed mineral sources (Suyanti et al., 2024; Allahkarami & Rezai, 2021). Therefore, developing improved

extraction systems specifically tailored for cerium is necessary to enhance recovery efficiency and meet industrial demand.

In industrial hydrometallurgical processes, acidic chloride media are commonly used for REE leaching due to their high solubility and compatibility with downstream separation techniques. Compared to other media, chloride systems offer advantages such as faster kinetics and easier phase separation (Afonin et al., 2024; Wei et al., 2020). However, extracting cerium from such environments still requires highly efficient and selective extractants.

Solvent extraction is the most widely applied technique for REE separation. Conventional single extractants, however, often suffer from limitations such as low extraction efficiency, poor selectivity, and operational issues including emulsion formation and extractant loss. Although previous studies have explored various extractants, there remains a need for more effective systems that can enhance cerium recovery under practical conditions (Lake et al., 2025; Merroune et al., 2024; Zhang et al., 2022).

To overcome these challenges, synergistic extraction using mixed extractants has emerged as a promising approach. This method enhances extraction efficiency, improves selectivity, and increases the stability of the organic phase, offering a more effective route for high-purity REE separation (Ning et al., 2025; Wei et al., 2020; Ghani et al., 2020) While this method has shown improved performance for general REE separation, its application specifically for cerium recovery in chloride media remains insufficiently explored. In particular, the synergistic interactions between ionic liquids and conventional extractants have not been fully investigated.

Therefore, this study focuses on evaluating the performance of selected synergistic extractant systems for the extraction of cerium from an acidic chloride solution. By comparing different binary extractant combinations, this work aims to identify an efficient and stable system that enhances cerium recovery and contributes to the development of improved separation technologies.

MATERIALS AND METHODS

Materials

Distilled kerosene and HCl solution (37%) were purchased from R&M Chemical Company. Tributyl phosphate (TBP), Di-(2-ethyl hexyl) phosphoric acid (D2EHPA), Trihexyl(tetradecyl)phosphonium bis(2,4,4-trimethylpentyl)phosphinate (Cyphos IL), Trioctylmethylammonium chloride (Aliquat 336) were four types of extractants selected for this research. All the other reagents were of analytical grade and used without further purification.

Methods

The rare earth chloride solution was prepared by dissolving an appropriate amount of the corresponding rare earth oxide powder in concentrated hydrochloric acid, followed by dilution with distilled water to the desired concentration. The organic phase was prepared by dissolving a specified amount of extractants in distilled kerosene under continuous stirring to ensure complete homogenization.

Extraction

Solvent extraction experiments were conducted in an acidic chloride medium (0.2 M) at room temperature (298 K) by contacting equal volumes (15 mL each) of the organic and aqueous phases, maintaining an organic-to-aqueous (O/A) phase ratio of 1:1. Synergist extractants between TBP, D2EHPA, Cyphos IL and Aliquat 336 was prepared as shown in Table 1. The mixtures were placed in covered Erlenmeyer flasks and vigorously agitated for 15 minutes using a mechanical shaker equipped with a magnetic stirrer to ensure that equilibrium was achieved. Following agitation, the phases were allowed to separate undisturbed for at least 10 minutes. Extraction experiments were performed in triplicate under identical conditions, and efficiencies are reported as mean ± standard deviation to ensure reproducibility.

Table 1: Synthesis of synergist extractants

Sample ID	Ratio	Extractant 1	Extractant 2
S01	-	TBP	-
S02	-	D2EHPA	-
S03	-	Aliquat 336	-
S04	-	Cyphos IL	-
S05	1:1	TBP	D2EHPA
S06	1:1	TBP	Aliquat 336
S07	1:1	TBP	Cyphos IL
S08	1:1	D2EHPA	Aliquat 336
S09	1:1	D2EHPA	Cyphos IL
S10	1:1	Aliquat 336	Cyphos IL

The concentrations of Ce(IV) in the aqueous phase, were determined using energy-dispersive X-ray fluorescence (ED-XRF). The extraction efficiency of Ce(IV), *E* was determined using Equation 1.

$$E(\%) = \frac{C_0 - C_e}{C_0} \times 100 \quad (1)$$

where C_o is the initial concentration of Ce in aqueous phase and C_e is the final concentration of Ce in aqueous phase after extraction.

RESULTS AND DISCUSSION

Extraction of Ce

The effect of varying extractants on cerium (Ce) extraction was investigated. The extraction process involves two immiscible phases: an aqueous phase containing rare earth elements (REEs) in an acidic chloride medium, and an organic phase comprising synergistic extractants. In this study, the organic phase utilized a combination of extractants, including TBP, D2EHPA, Cyphos IL, and Aliquat 336. These extractants were selected based on their known affinities for lanthanides and compatibility with acidic chloride media. The efficiency of Ce extraction between different extractants are shown in Table 2.

Table 2: Extraction efficiency of Ce using TBP, D2EHPA, Cyphos IL, and Aliquat 336

Sample ID	Extraction	Efficiency of Ce extraction
S01	Single	2.44
S02	Single	46.2
S03	Single	39.7
S04	Single	73.2
S05	Synergist	70.7
S06	Synergist	42.0
S07	Synergist	66.2
S08	Synergist	51.6
S09	Synergist	94.1
S10	Synergist	51.2

As shown in Table 2, the individual extractants exhibited moderate extraction efficiencies when employed separately. Among them, D2EHPA (S02) displayed enhanced selectivity toward Ce, relative to TBP (S01) and Aliquat 336 (S03), likely due to its strong cation-exchange properties. Remarkably, the combination of D2EHPA with Cyphos IL (S09) in a synergistic extraction system significantly improved the extraction efficiency, reaching up to 94.1% under ambient conditions, followed by TBP/D2EHPA (S05), TBP/Cyphos IL (S07), D2EHPA/Aliquat 336 (S08), Aliquat 336/Cyphos IL (S10) and TBP/Aliquat 336 (S06) as illustrated in Figure 1.

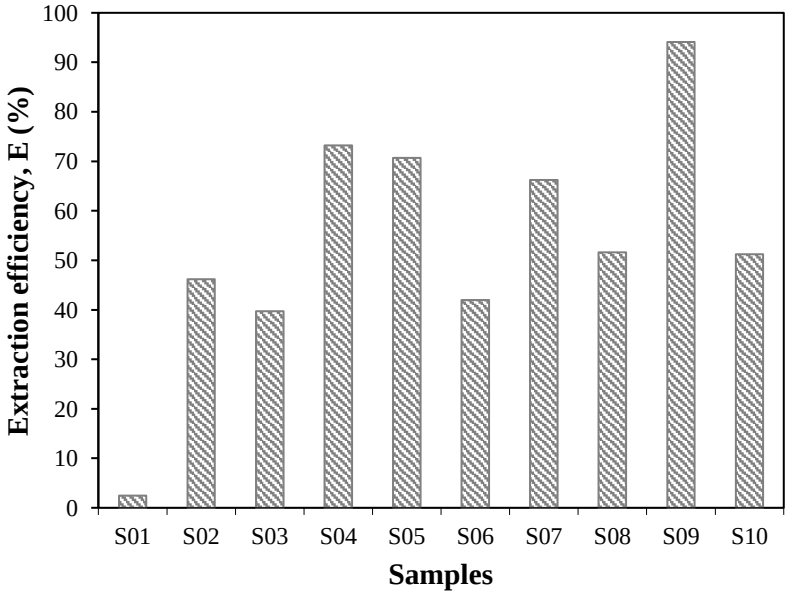

Figure 1: Extraction efficiency of Ce using TBP, D2EHPA, Cyphos IL, and Aliquat 336 [Fixed conditions: T= room temperature; O/A ratio = 1/1]

The improved extraction efficiency of the D2EHPA/Cyphos IL (S09) system is attributed to a synergistic interaction between the acidic organophosphorus extractant and the ionic liquid. D2EHPA facilitates the extraction of Ce^{3+} via a proton exchange mechanism, while Cyphos IL enhances the solvation and stabilization of the extracted metal complex, thereby promoting favorable phase transfer kinetics and increasing the metal-loading capacity. The combined action of both components reduces interfacial tension, leading to more efficient partitioning of Ce^{3+} into the organic phase.

No significant third-phase formation was observed, as confirmed by visual inspection of the phases, indicating good phase compatibility and stability of the extractant system under the tested conditions. Furthermore, the D2EHPA/Cyphos IL (S09) system demonstrated selective extraction of Ce over other lanthanides present in the leachate, such as La and Nd, under the same experimental conditions. This selectivity is advantageous for downstream separation and purification processes.

CONCLUSION

Rare earth chlorides were successfully extracted from monazite mineral via solvent extraction. Laboratory-scale studies demonstrated that Ce could be efficiently recovered from an acidic chloride medium using synergistic extractant systems. Among the extractants evaluated, the combination of D2EHPA and Cyphos IL exhibited the highest extraction efficiency for cerium, achieving 94.1%. The synergistic system outperformed individual extractants under ambient conditions, indicating a significant enhancement in extraction performance through synergism.

ACKNOWLEDGEMENTS

This research was supported by the Ministry of Science, Technology and Innovation (MOSTI) of Malaysia through DSTIN Thorium Flagship Fund - Development of Innovative Nuclear Reactor Technology (with the Spin-Off) Based on Thorium (2015 - 2019). This research paper also was a part of the PQRD project (NM-R&D-21-77) entitled “Synergistic Solvent Extraction of Cerium from Monazite Mineral”.

REFERENCES

Afonin, M.A., Nechaev, A.V., Yakimenko, I.A. & Belova, V.V. (2024). Extraction of rare earth elements from chloride solutions using mixtures of p507 and cyanex 272. *Compounds*, 4, 172-181. https://doi.org/10.3390/compounds4010008

Allahkarami, E. & Rezai, B. (2021). A literature review of cerium recovery from different aqueous solutions. *Journal of Environmental Chemical Engineering*, 9(1), 104956. https://doi.org/10.1016/j.jece.2020.104956

Balaram, V. (2019). Rare earth elements: a review of applications, occurrence, exploration, analysis, recycling, and environmental impact. *Geoscience Frontiers*, 10, 1285-1303. https://doi.org/10.1016/j.gsf.2018.12.005

Ghani, L., Shahida, S., Khan, M.H., Aziz, B., Masood, M., Badshah, S.L. & Khan, M. (2020). Liquid–liquid extraction of Eu(lll) using synergic mixture of 1-phenyl-3-methyl-4-trifluoroacetyl-2-pyrazolin-5-one and crown ethers. *SN Applied Sciences*, 2, 1541. https://doi.org/10.1007/s42452-020-03337-2

Hamzat, A.K., Murad, M.S., Subeshan, B. & Asmatulu, R. (2025). Rare earth element recycling: a review on sustainable solutions and impacts on semiconductor and chip industries. *Journal of Material Cycles and Waste Management*, 27, 3009-3032. https://doi.org/10.1007/s10163-025-02276-7

Lake, B., Siegrist, T., Albrecht, T.E., Mohammadigoushki, H., Humayun, M. & Ali, J. recent advances in rare earth element recovery: liquid–liquid extraction and magnetophoretic separation. *Industrial & Engineering Chemistry Research,* 64(41), 19781-19796. https://doi.org/10.1021/acs.iecr.5c02137

Merroune, A., Brahim, J.A., Berrada, M., Essakhraoui, M., Achiou, B., Mazouz, H. & Beniazza, R. (2024). A comprehensive review on solvent extraction technologies of rare earth elements from different acidic media: Current challenges and future perspectives. *Journal of Industrial and Engineering Chemistry*, 139, 1-17. https://doi.org/10.1016/j.jiec.2024.04.042

Ning, K., Wang, J., Zhang, J., Hong, M., Fu, B., Deng, J., Gui, X., Xing, Y., Fan, G. & Xu, H. (2025). The separation of y and er based on the synergistic effect of [N1444][P507] and TRPO. *Minerals*, 15(153), 1-17. https://doi.org/10.3390/min15020153

Suyanti, Pusporini, N.D., Adi, W.A., Petrus, H.T.B.M. (2024). Characteristics and performance of cerium extraction from cerium hydroxide concentrate using tri butyl phosphate. *International Journal of Technology*,15(5), 1308-1320. https://doi.org/10.14716/ijtech.v15i5.6010

Wei, H., Li, Y., Zhang, Z. & Liao, W. (2020). Synergistic solvent extraction of heavy rare earths from chloride media using mixture of HEHHAP and Cyanex272. *Hydrometallurgy,* 191(105241), 1-7. https://doi.org/10.1016/j.hydromet.2019.105240

Zhang, W., Feng, D., Xie, X., Tong, X., Du, Y. & Cao, Y. (2022). Solvent extraction and separation of light rare earths from chloride media using HDEHP-P350 system. *Journal of Rare Earths*, 40(2), 328-337. https://doi.org/10.1016/j.jre.2021.05.003

Jurnal Sains Nuklear Malaysia, 2026, 38(Special Issue): 43 – 52
ISSN: 2232-0946

CHARACTERIZATION OF GAMMA-IRRADIATED CALCIUM SILICATES FROM GLASS WASTE

Ahmad Hasnulhadi C.K.[1*], Muhammad Danial Arif M.Z.[2], Wilfred P. [3] and Nur Ubaidah S. [3]

[1]Waste Technology Development Centre, Waste and Environmental Technology Division,
43000 Kajang, Selangor, Malaysia
[2]Faculty of Science and Marine Environment, Universiti Malaysia Terengganu,
21300 Kuala Terengganu, Terengganu, Malaysia
[3]Material Technology Group, Industrial Technology Division,
43000 Kajang, Selangor, Malaysia
*Correspondence author: hadi@nm.gov.my

ABSTRACT

With the rising concern over industrial glass waste, there is a growing need to develop sustainable strategies for material reuse. This study explores the potential of recycled calcium silicate ($CaSiO_3$) nano glass slides as eco-friendly and radiation-tolerant materials. The research focused on synthesizing ultrafine $CaSiO_3$ nanomaterials from used glass slides and evaluating their structural and morphological responses to gamma irradiation from a Cobalt-60 (Co-60) source. To assess these characteristics, three main analytical techniques were employed: X-ray Fluorescence (XRF) to determine elemental composition, X-ray Diffraction (XRD) to examine crystallographic structure, and Field Emission Scanning Electron Microscopy coupled with Energy Dispersive X-ray Spectroscopy (FESEM-EDX) to study surface morphology and elemental distribution. XRF analysis confirmed calcium and silicon as the primary elements in the recycled samples, along with minor impurities likely introduced during processing. XRD results showed that as radiation doses increased (from 20 to 70 kGy), diffraction peaks became broader and less intense, indicating progressive structural disorder, though the fundamental crystal phase remained intact. FESEM-EDX imaging further revealed notable changes in the surface structure, including increased particle agglomeration and grain growth corresponding to higher radiation exposure. Overall, the study demonstrates that recycled $CaSiO_3$ nano glass retains its chemical and structural integrity even after significant gamma irradiation. These results highlight the material's promise for use in radiation-exposed environments, offering a meaningful step forward in transforming glass waste into valuable, sustainable nanomaterials suitable for environmental and industrial applications.

Keywords: Recycled Calcium Silicate ($CaSiO_3$); Gamma Irradiation; X-ray Diffraction (XRD); X-ray Fluorescence (XRF); Field Emission Scanning Electron Microscopy (FESEM-EDX)

INTRODUCTION

The growing volume of industrial and household glass waste worldwide necessitates a thorough examination of sustainable recycling methods to enhance the value of these materials. An effective approach involves converting waste glass into functional ceramic compounds, such as calcium silicate ($CaSiO_3$), with diverse applications in biomedical, environmental, and radiation-related fields. This sustainable and cost-effective method reduces landfill pressure and promotes material circularity by utilizing waste streams rich in silicates.

Numerous studies have explored the effects of ionizing radiation, particularly gamma rays, on the structure, heat, and light properties of silicate-based materials. For instance, Baltac and Mitran (2025) conducted a detailed analysis of gamma irradiation's impact on silica-based nanomaterials, highlighting changes in crystal structures and surface reactivity. Similarly, Büyükuslu et al. (2022) observed significant alterations in the morphology and luminescent properties of Nb-doped TiO_2 nanoparticles post-irradiation, indicating the formation of radiation-induced defects. The investigation of calcium silicate ceramics has attracted considerable academic interest due to their biocompatibility and responsiveness to radiation exposure.

Rare earth-doped polycrystalline $CaSiO_3$, synthesized by Gonzales-Lorenzo et al. (2018, 2020), shows promise for photon and neutron detection through thermoluminescence. The bioactivity and interfacial bonding of calcium silicates, as discussed by Hench et al. (1971) and Lin et al. (2007), suggest their suitability for biomedical scaffolds. Hao et al. (2018) demonstrated the significant sorption capacity of $CaSiO_3$ composites derived from industrial slag for removing hazardous metal ions in aquatic environments.

Despite extensive research on synthetic $CaSiO_3$ properties and its response to radiation, there is a lack of studies on utilizing recycled glass to produce $CaSiO_3$ nanomaterials and investigating the effects of Co-60 gamma irradiation on their structure and morphology. This gap presents a crucial area for advancing sustainable materials for nuclear and environmental applications.

This study aims to synthesize ultrafine calcium silicate ($CaSiO_3$) nanomaterials from used glass slides and examine how Co-60 gamma radiation influences their structure and morphology. Analytical characterizations using X-ray Fluorescence (XRF), X-ray Diffraction (XRD), and Field Emission Scanning Electron Microscopy with Energy Dispersive X-ray Spectroscopy (FESEM-EDX) were employed to determine composition, crystallinity, and surface morphology.

MATERIALS AND METHODS

Preparation of $CaSiO_3$ Glass Nanomaterials

Figure 1 illustrates the preparation of nano $CaSiO_3$ powder using the dry processing technique. It starts with the collection of discarded glass slides, which are then cleaned with distilled water to remove any surface residues or contaminants. This cleaning stage is crucial to eliminate any dirt that may affect the subsequent characterization process. After the cleaning process, the slides are manually ground using a mortar and pestle, reducing their size. This grinding is followed by ball milling technique to further crush the $CaSiO_3$ sample into finer particles. The mortar and pestle ensure efficient and controlled glass fragmentation, while the ball mill ensures that the sample size becomes finer, enhancing the uniformity of the powder at the ultrafine level. The sieved $CaSiO_3$ powder is then ready for characterization, a crucial step before exposure to Co-60 gamma radiation. The prepared nano material serves as a basis for analyzing structural and morphological changes after irradiation.

Figure 1: Preparation of $CaSiO_3$ Glass Nanomaterials before exposure

Characterization Techniques

X-ray Diffraction (XRD)

For XRD analysis, $CaSiO_3$ was ground and spread onto the sample holder to obtain a homogeneous surface area. The diffraction patterns were recorded using a Panalytical X'Pert PRO X-ray diffractometer (XRD) as shown in Figure 2 to analyse the structural properties of recycled nano $CaSiO_3$ glass slides before and after Co-60 gamma irradiation. This analysis was performed to confirm and evaluate changes in crystallinity, structural stability, and peak intensity in the samples after gamma irradiation. This analysis is crucial for evaluating its suitability in sustainable and radiation-resistant material applications.

Figure 2: Panalytical, X'Pert Pro

Field Emission Scanning Electron Microscopy with Energy Dispersive X-ray Spectroscopy (FESEM-EDX)

For FESEM-EDX analysis, the powder samples were mounted on a carbon tape and sputter-coated to reduce surface charging during image acquisition. The samples were observed using a Carl Zeiss/GeminiSEM 500 as shown in Figure 3 to assess physical features of $CaSiO_3$ samples before and after exposure to Co-60 gamma radiation, including particle size, morphology, surface texture, and agglomeration behavior of nanoscale particles, which are critical factors in assessing the quality and performance of materials. At the same time, EDX analysis was used to verify the elemental distribution on the sample surface.

Figure 3: Carl Zeiss/GeminiSEM 500

X-ray Fluorescence (XRF)

XRF is a non-destructive technique that was used to determine the elemental composition of a material. When the sample is irradiated with primary X-rays, electrons are ejected from the inner shell, which emit secondary X-rays. The emitted X-rays were used to identify the sample elements and measure their concentrations before and after irradiation.

It also detects any trace amounts of other substances, such as impurities or unwanted materials, that may have entered the glass during the recycling process. Understanding this information helps us assess whether the recycled glass retains good quality and is similar to the original, or if any changes could affect its functionality.

In this study, XRF was used to determine the elemental concentrations of recycled CaSiO3 nano-glass before and after irradiation. The powder samples were cleaned, placed in the sample holder, and then analyzed using a Shimadzu EDX-7000 spectrometer under ambient conditions. To ensure the reliability of elemental analysis measurements, the equipment was calibrated with appropriate reference standards.

Figure 4 shows a specialized machine called an X-ray Fluorescence (XRF) spectrometer used in this experiment. This machine helps to determine the types of small elements (such as atomic components) in the recycled calcium silicate nanoglass slide. An interesting thing about XRF is that it does not harm the sample; it only emits strong X-rays onto it. These X-rays cause the atoms in the sample to emit their own small X-ray signals. By analyzing these signals, scientists can identify which elements are present in the sample and how much of each element is present.

Overall, XRF analysis provided valuable insights into the elemental composition and purity of the recycled $CaSiO_3$ nano glass slides, supporting the evaluation of the recycling process's effectiveness and consistency for reuse in scientific or industrial applications.

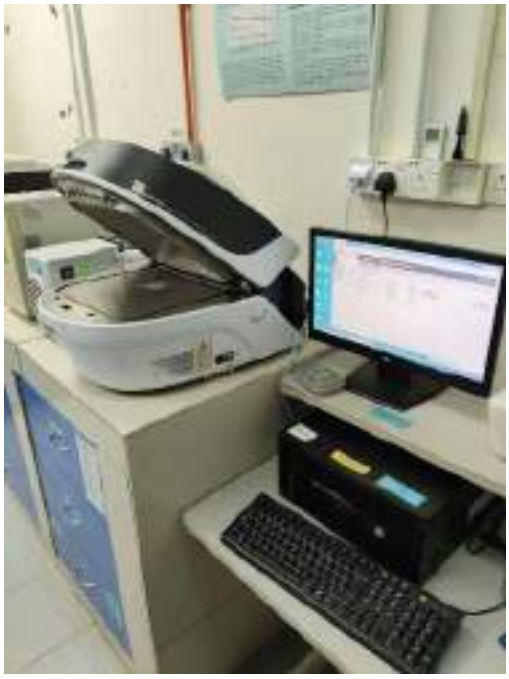

Figure 4: Shimadzu / EDX7000

Data collection

The data collection process will consist of two main steps: pre-radiation exposure and post-radiation exposure. Initially, the $CaSiO_3$ nanomaterials will undergo thorough examination through various tests before any radiation exposure. These tests will include radiation detectors to measure initial radiation levels, Energy Dispersive X-Ray Fluorescence (EDXRF) to determine elemental composition, FESEM-EDX to analyze surface morphology, and X-Ray Diffraction (XRD) to study crystal structure. These tests will provide a comprehensive understanding of the material's properties prior to radiation exposure.

Subsequently, the recycled $CaSiO_3$ nanomaterials will be subjected to gamma rays emitted from a Cobalt-60 (Co-60) source to observe the effects of high-energy radiation on the material. The same tests, FESEM-EDX and XRD, will be repeated post-radiation exposure to compare any structural or surface changes that may have occurred.

RESULTS AND DISCUSSION

XRF Analysis

Table 1 presents the XRF analysis results for $CaSiO_3$ samples pre-gamma irradiation. Silicon (Si) and calcium (Ca) were the predominant elements, comprising approximately 58.7% and 37.0% of the composition, respectively. These concentrations align with the expected stoichiometry of $CaSiO_3$, confirming successful compound formation. Minor elements like potassium (K), iron (Fe), sulfur (S), chlorine (Cl), silver (Ag), titanium (Ti), and others were detected in trace amounts (<2%), likely originating from feedstock recycling or processing contamination. The presence of high-energy characteristic peaks, such as Si Kα (1.74 keV) and Ca Kα (3.70 keV), ensured accurate elemental identification. Understanding the elemental distribution is crucial for assessing the suitability of recycled materials for high-performance applications, particularly in radiation environments.

Table 1: XRF results for $CaSiO_3$ samples before exposure

Analytical	Concentration (%)	Analytical	Energy (keV)
Si	58.732	Si Kα	1.74
Ca	37.048	Ca Kα	3.70
K	1.629	K Kα	3.32
Fe	1.029	Fe Kα	6.40
S	0.699	S Kα	2.30
Cl	0.274	Cl Kα	2.62
Ag	0.145	Ag Kα	22.02
Ti	0.143	Ti Kα	4.52
Mn	0.093	Mn Kα	5.90
Cr	0.067	Cr Kα	5.42
Sr	0.063	Sr Kα	14.16
Cu	0.040	Cu Kα	8.06
Rb	0.023	Rb Kα	13.36
Zn	0.016	Zn Kα	8.66

XRD Analysis

Figure 5(a) displays the XRD patterns of $CaSiO_3$ samples in grounded and ultra-grounded states. The ultra-grounded sample revealed sharper diffraction peaks, notably around 25° and 43°, indicating improved crystallinity. Both samples exhibited broad humps within 10°–35°, suggesting an amorphous phase presence, consistent with previous findings (Gimenez-Carbo et al., 2021). The detected phases were assigned to SiO_2, $CaCO_3$, and $CaSiO_3$, which should be indicated in the figure legend for clarity.

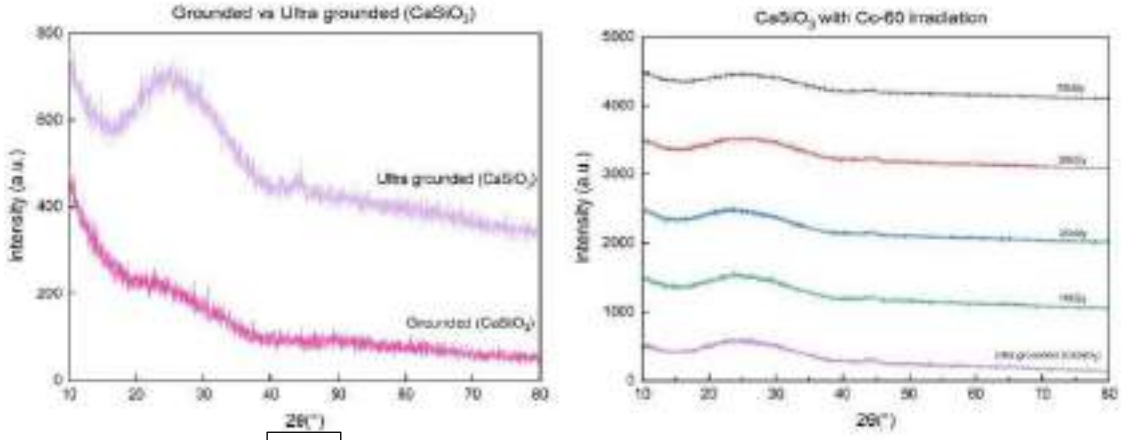

Figure 5 (a): XRD patterns of ground and ultra-ground $CaSiO_3$ samples
Figure 5 (b) shows the XRD patterns of $CaSiO_3$ after Co-60 gamma irradiation at doses ranging from 0 to 70 kGy.

As the irradiation dose increased, the diffraction peaks became broader and less intense, while the background signal gradually increased. These features suggest a reduction in crystallinity and the formation of radiation-induced defects, although the main crystalline phase remained detectable throughout the dose range studied, as previously observed in similar materials (Gonzales-Lorenzo et al., 2018).

FESEM Morphology and Particle Size Analysis

Table 2 and Table 3 present SEM images and average particle sizes of $CaSiO_3$ samples before and after gamma irradiation. Pre-irradiation samples showed rough, porous, and irregular particles. At 20 kGy, increased grain compaction and clustering were observed. By 30 and 40 kGy, partial sintering, smoothing, and densification became more evident. At 70 kGy, larger and more compact particles indicated significant radiation-induced diffusion and agglomeration.

Table 2: FESEM figures for $CaSiO_3$ samples before and after exposure

Magnification / **Radiation range**	**5kx**	**10kx**	**20kx**
Grounded	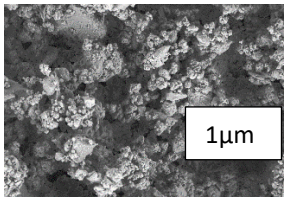	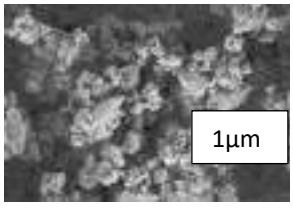	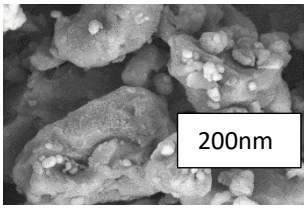
20 kGy	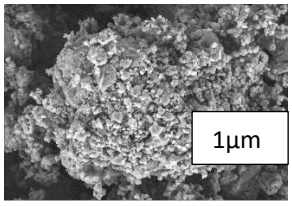	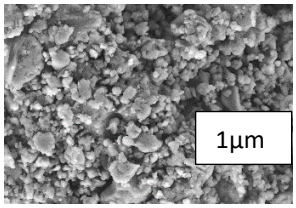	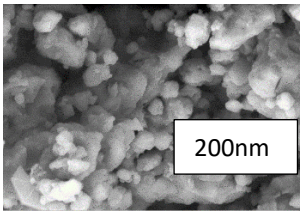

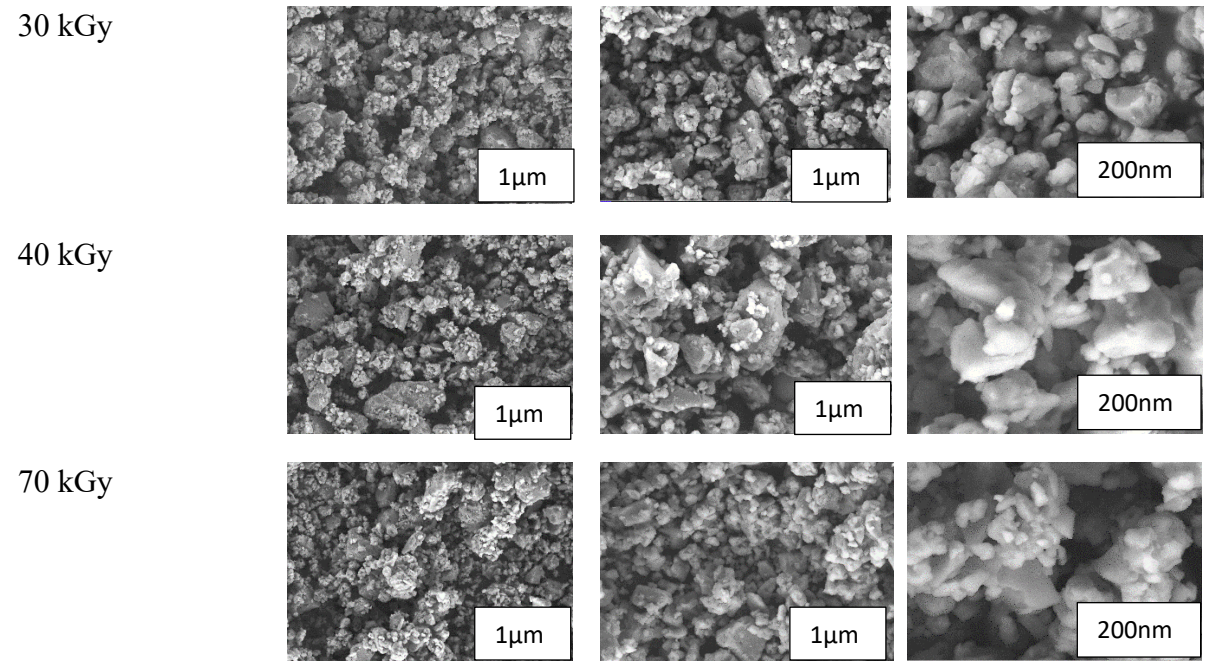

Table 3: Particle size distribution of $CaSiO_3$ samples measured at 20kx magnification

Magnification	**Control (µm)**	**20kGy (µm)**	**30kGy (µm)**	**40kGy (µm)**	**70kGy (µm)**
20kx	0.107	0.166	0.151	0.170	0.180

Table 3 summarises the particle sizes measured at 20kx magnification for the control and irradiated samples. The average particle size increased from 0.107 µm in the control sample to 0.166 µm after irradiation at 20 kGy, indicating initial agglomeration. The values at 30 and 40 kGy were 0.151 µm and 0.170 µm, respectively, while the 70 kGy sample showed the largest particle size of 0.180 µm. These results align with observed FESEM morphology and confirm gamma irradiation influences microstructure significantly.

CONCLUSION

The first objective was successfully achieved through this study: ultrafine calcium silicate ($CaSiO_3$) nanomaterials were synthesized from recycled glass slides via dry mechanical processing, including ball milling. The resulting gray powder showed sufficient fineness and homogeneity for further material testing.

Second, structural and morphological characterization confirmed the properties of the synthesized materials as expected. FESEM analysis revealed that the unirradiated sample consisted of irregular, porous particles with rough surfaces. Upon exposure to increasing doses of gamma radiation (20–70 kGy), the particles showed enhanced density, reduced porosity, and gradual grain growth with particle sizes at 20kx magnification increasing overall from 0.107 µm in the control sample to 0.180 µm at 70 kGy.

Third, the effect of Co-60 gamma irradiation was examined by XRD spectroscopy. The XRD pattern showed sharper peaks in the irradiated samples, indicating increased crystallinity.

In summary, this study demonstrated that recycled glass slides can be effectively modified into structurally stable $CaSiO_3$ nanomaterials. The materials exhibited durability under gamma irradiation, maintaining phase integrity and functional morphology. These findings support the potential use of recycled $CaSiO_3$ in radiation-resistant materials for environmental and industrial technologies.

ACKNOWLEDGEMENTS

The authors gratefully acknowledge Nuklear Malaysia and Universiti Malaysia Terengganu (UMT), particularly the WasTeC, MTEG and ACA groups, as well as the dedicated supervisors and laboratory personnel, for their invaluable technical support and guidance throughout this research project.

REFERENCES

Baltac, A. S., & Mitran, R. (2025). Gamma radiation in the Synthesis of Inorganic Silica-Based nanomaterials: a review. *Nanomaterials*, *15*(3), 218. https://doi.org/10.3390/nano15030218

Boizot, B., Petite, G., Ghaleb, D., Reynard, B., & Calas, G. (1999). Raman study of β-irradiated glasses. *Journal of Non-Crystalline Solids*, *243*(2–3), 268–272. https://doi.org/10.1016/s0022-3093(98)00822-9

Büyükuslu, H., Kutlu, N., & Kaya, S. (2022). Influences of gamma irradiation on structural, morphological and luminescence characteristics of Nb doped TiO2 nanophosphors. *Nuclear Instruments and Methods in Physics Research Section B Beam Interactions with Materials and Atoms*, *535*, 234–240. https://doi.org/10.1016/j.nimb.2022.12.016

Dong, W., Li, W., & Tao, Z. (2021). A comprehensive review on performance of cementitious and geopolymeric concretes with recycled waste glass as powder, sand or cullet. *Resources Conservation and Recycling*, *172*, 105664. https://doi.org/10.1016/j.resconrec.2021.105664

Gimenez-Carbo, E., Soriano, L., Roig-Flores, M., & Serna, P. (2021). Characterization of Glass Powder from Glass Recycling Process Waste and Preliminary Testing. *Materials*, *14*(11), 2971. https://doi.org/10.3390/ma14112971

Gonzales-Lorenzo, C. D., Watanabe, S., Cano, N. F., Ayala-Arenas, J. S., & Bueno, C. C. (2018). Synthetic polycrystals of CaSiO3 un-doped and Cd, B, Dy, Eu-doped for gamma and neutron detection. *Journal of Luminescence*, *201*, 5–10. https://doi.org/10.1016/j.jlumin.2018.04.037

Gonzales-Lorenzo, C. D., Nascimento, L. F., Kodaira, S., Gomes, M. B., & Watanabe, S. (2020). Thermoluminescence studies of polycrystalline CaSiO3 pellets for photons and particle therapy beams. *Radiation Physics and Chemistry*, *177*, 109132. https://doi.org/10.1016/j.radphyschem.2020.109132

Hench, L. L., Splinter, R. J., Allen, W. C., & Greenlee, T. K. (1971). Bonding mechanisms at the interface of ceramic prosthetic materials. *Journal of Biomedical Materials Research*, *5*(6), 117–141. https://doi.org/10.1002/jbm.820050611

Jiménez, J. A., & Crawford, C. L. (2023). Raman and optical spectroscopy study of iron-bearing bio-relevant phosphate glasses: Assessment of γ-ray irradiation effects. *Chemical Physics*, *569*, 111854. https://doi.org/10.1016/j.chemphys.2023.111854

Li, R., Yang, W., Gao, S., Shang, J., & Li, Q. (2021). Hydrous cerium oxides coated glass fiber for efficient and long-lasting arsenic removal from drinking water. *Journal of Advanced Ceramics*, *10*(2), 247–257. https://doi.org/10.1007/s40145-020-0435-0

Lin, K. L., Ni, S. Y., Chang, J., Zhai, W. Y., & Gu, W. M. (2007). Fabrication and Characterization of Bioactive Glass Reinforced $CaSiO_3$ Ceramics. *Key Engineering Materials*, *330–332*, 181–184. https://doi.org/10.4028/www.scientific.net/kem.330-332.181

Moreno-Santos, A., Rios-Hurtado, J. C., Flores-Villaseñor, S. E., Esmeralda-Gomez, A. G., Guevara-Chavez, J. Y., Lara-Castillo, F. P., & Escalante-Ibarra, G. B. (2022). Hydroxyapatite growth on activated carbon surface for methylene blue adsorption: effect of oxidation time and CASIO3 addition on hydrothermal incubation. *Applied Sciences*, *13*(1), 77. https://doi.org/10.3390/app13010077

Obayes, H. K., Wagiran, H., Hussin, R., Saeed, M. A., & Saidu, A. (2015). Thermoluminescence Response of Nanoparticles Gold Doped Lithium Borate Glass Subjected to Photon Irradiation. *Jurnal Teknologi*, *77*(1). https://doi.org/10.11113/jt.v77.3676

Qiu, B., Duan, X., Zhang, Z., Zhao, C., Niu, B., He, P., Cai, D., Chen, L., Yang, Z., Wang, Y., Jia, D., & Zhou, Y. (2021). Microstructural evolution of h-BN matrix composite ceramics with La-Al-Si-O glass phase during hot-pressed sintering. *Journal of Advanced Ceramics*, *10*(3), 493–501. https://doi.org/10.1007/s40145-020-0451-0

Rai, V. N., Sekhar, B. N. R., & Jagtap, B. N. (2014). Study of gamma induced defects in Nd doped phosphate glass using UV-Vis spectrophotometer and photophysics beamline on INDUS-1. *arXiv (Cornell University)*. https://doi.org/10.48550/arxiv.1406.7717

Siriphannon, P., Kameshima, Y., Yasumori, A., Okada, K., & Hayashi, S. (2002). Formation of hydroxyapatite on CaSiO3 powders in simulated body fluid. *Journal of the European Ceramic Society*, *22*(4), 511–520. https://doi.org/10.1016/s0955-2219(01)00301-6

Shao, N., Tang, S., Liu, Z., Li, L., Yan, F., Liu, F., Li, S., & Zhang, Z. (2018). Hierarchically Structured Calcium Silicate Hydrate-Based Nanocomposites Derived from Steel Slag for Highly Efficient Heavy Metal Removal from Wastewater. *ACS Sustainable Chemistry & Engineering*, *6*(11), 14926–14935. https://doi.org/10.1021/acssuschemeng.8b03428

Zhang, M., Xia, X., Cao, C., Xue, H., Yang, Y., Li, W., Chen, Q., Xiao, L., & Qian, Q. (2020). A ZnO@ABS/TPU/CaSiO3 3D skeleton and its adsorption/photocatalysis properties for dye contaminant removal. *RSC Advances*, *10*(68), 41272–41282. https://doi.org/10.1039/d0ra06661c

Zhu, S., Sun, Y., Pan, Y., Chen, X., Bai, K., Wang, Y., Yang, F., Qin, K., Mao, J., Zhang, X., Wang, T., & Peng, H. (2023). Radiation effects of B depletion and the generation of point defects in ternary borosilicate glasses by gamma rays. *Journal of Non-Crystalline Solids*, *619*, 122576. https://doi.org/10.1016/j.jnoncrysol.2023.122576

Jurnal Sains Nuklear Malaysia, 2026, 38(Special Issue): 53 – 61
ISSN: 2232-0946

SYNTHESIS AND CHARACTERIZATION OF CERIUM OXIDE NANOPARTICLES VIA PRECIPITATION–CALCINATION METHOD

Cik Rohaida Che Hak[1*] and Siti Aisyah Aqilah Mohd Azny[2]

[1]Industrial Technology Division, Agensi Nuklear Malaysia, Bangi,
43000 Kajang, Selangor, Malaysia.
[2]Faculty of Applied Science, Universiti Teknologi MARA, Cawangan Perlis, Arau, Perlis
*Correspondence author: rohaida@nm.gov.my

ABSTRACT

Cerium is classified as a rare earth element suitable in many industrial applications. Cerium oxide (CeO_2), in particular has been widely used as catalysts in the petrochemical industries. Recently, CeO_2 has been investigated for its potential in sensor technology application, especially in biosensing. In this study, nanoporous CeO_2 was successfully synthesized through a precipitation -calcination route using cerium (IV) sulfate hydrate as a precursor. The synthesis involved pH-controlled precipitation at room temperature using ammonium hydroxide as the precipitation agent. The solid precipitate was separated from the excess liquid and dried overnight in an oven. The precipitate was then calcined at 600°C for 2 hours. Structural and morphological characterization was performed using Fourier Transform Infrared Spectroscopy (FTIR) and Field Emission Scanning Electron Microscopy (FESEM). FTIR analysis confirmed that the synthesis converted the hydroxide-sulfate precursor to CeO_2, as evidenced by the disappearance of sulfate bands and the emergence of Ce-O lattice vibrations. FESEM imaging revealed a nanoporous morphology with uniform particle distribution. Elemental compositional analysis via Energy Dispersive X-ray Spectroscopy (EDX) confirmed the presence of Ce with minimal residual sulfur contamination, while X-Ray diffraction (XRD) analysis exhibited the formation of CeO_2 phase. The synthesis yielded an 85% mass retention, demonstrating the potential of this route for efficient production of high-purity CeO_2.

Keywords: cerium oxide, nanoparticles, precipitation-calcination, thermal decomposition

Abstrak

Cerium dikelaskan sebagai sejenis unsur nadir bumi yang sesuai untuk pelbagai aplikasi industri. Khususnya, cerium oksida (CeO_2) telah digunakan secara meluas sebagai pemangkin di dalam industri petrokimia. Terkin CeO_2 telah dikaji akan potensinya dalam aplikasi teknologi penderiaan, terutamanya dalam penderiaan bio. Dalam kajian ini, CeO_2 berliang nano telah berjaya disintesis melalui laluan pemendakan-pengkalsinan dengan menggunakan cerium (IV) sulfat terhidrat sebagai bahan pemula. Sintesis ini melibatkan pemendakan terkawal pH pada suhu bilik menggunakan ammonium hidroksida sebagai ejen pemendakan. Mendakan pepejal tersebut dipisahkan daripada lebihan cecair dan dikeringkan semalaman di dalam ketuhar. Mendakan itu kemudiannya dikalsinkan pada suhu 600°C selama 2 jam. Pencirian struktur dan morfologi telah dijalankan menggunakan Spektroskopi Inframerah Transformasi Fourier (FTIR) dan Mikroskop Elektron Imbasan Pancaran Medan (FESEM). Analisis FTIR mengesahkan bahawa sintesis tersebut telah menukarkan bahan pemula hidroksida-sulfat kepada CeO_2, seperti yang dibuktikan melalui kehilangan jalur sulfat dan kemunculan getaran kekisi Ce-O. Imej FESEM mendedahkan morfologi berliang nano dengan taburan zarah yang seragam. Analisis komposisi unsur melalui Spektroskopi Sinar-X Serakan

Tenaga (EDX) mengesahkan kehadiran Ce dengan pencemaran sisa sulfur yang minimum, manakala analisis Belauan Sinar-X (XRD) menunjukkan pembentukan fasa CeO_2. Sintesis ini menghasilkan pengekalan jisim sebanyak 85%, menunjukkan kecekapan laluan ini berpotensi untuk menghasilkan CeO_2 dengan ketulenan tinggi.

INTRODUCTION

In the last several years, Ce-based compounds have received attention because of their widespread applications in industrial applications (Dahle & Arai, 2015). Cerium's unique electronic configuration specifically the 4f electrons shielded by 5s and 5p orbitals, contributes to its chemical versatility and enables variable valence reactions (Campbell & Peden, 2005). In addition, the ability of cerium to transition between Ce^{3+} and Ce^{4+}oxidation states generates oxygen vacancies that facilitate various catalytic processes (Campbell & Peden, 2005). Cerium oxide (CeO_2) particularly, has been extensively studied for its role in oxidation-reduction reactions, making it a critical material in automotive catalytic converters and solid oxide fuel cells (Sun et al., 2012). Recent advancements in nanotechnology have further enhanced the interest in CeO_2 nanoparticles for biomedical use, owing to their "nanozyme" activities, including peroxidase-, superoxide dismutase-, and catalase-like reactions (Das et al., 2013, Zhan et al., 2012, Mahmoud et al., 2022). These properties make CeO_2 nanoparticles (NPs) excellent candidates for biosensing applications, offering dual-mode detection capabilities with sub-picogram sensitivity (Wang et al., 2024).

Cerium (Ce) is one of the rare earth elements (REEs) belonging to the lanthanide series, and is the most abundant rare earth element in the Earth's crust It is commonly found in minerals such as monazite and bastnäsite (Gupta&Krishnamurthy, 2005). In addition to Ce, Malaysian monazite contains several other rare earth elements, including Lanthanum (La), Neodymium (Nd), Praseodymium (Pr), Samarium (Sm), and others. Monazite is also contaminated with thorium, a naturally occurring radioactive material, which raises radiological concerns and limits its applications. Furthermore, the extraction of CeO_2 from monazite involves multiple processing steps, including acid digestion, extensive separation of cerium from other rare earth elements, and complex solvent extraction procedures for purification. These processes are time-consuming and may take several weeks to months to complete.

Owing to these limitation, this study investigates the potential of synthesis CeO_2 NPs via a simple precipitation-calcination method. Various synthesis routes for CeO_2 NPs have been reported, including chemical precipitation-calcination (Pouretedal & Kadkhodaie, 2010), sol-gel (Alifanti et al., 2003), thermal decomposition (Wang et al., 2002), hydrothermal (Phoka et al., 2012), and combustion method (Bojana et al., 2008). Among these approaches, precipitation-calcination remains the predominant method due to its simplicity, scalability, and cost-effectiveness (Dahle & Arai, 2015). In this study cerium (IV) sulfate hydrate has been chosen as the precursor, owing to its high solubility, well-defined hydration states, and predictable thermal decomposition pathway. A straightforward synthesis route for CeO_2 NPs was developed through controlled precipitation followed by calcination. The structural evolution from precursor to final oxide and the morphological characteristics of the resulting NPs were characterized using FTIR spectroscopy and electron microscopy. The formation of CeO_2 after calcination was confirmed using X-ray diffraction (XRD).

MATERIALS AND METHODS

Materials

Cerium(IV) sulfate hydrate ($Ce(SO_4)_2 \cdot xH_2O$), ammonium hydroxide (25% NH_4OH), and distilled water were used as received without further purification. All chemicals were of analytical grade.

Synthesis Procedure

The synthesis was carried out following a modified chemical precipitation-calcination method (Krystof & Ondrejl, 2019). Cerium(IV) sulfate hydrate (3.25 g) was dissolved in 5 mL of distilled water under vigorous magnetic stirring until complete dissolution. Ammonium hydroxide solution (25%) was added dropwise under continuous pH monitoring until precipitation occurred The resulting precipitate was separated by vacuum filtration and washed repeatedly with distilled water to remove residual ammonium sulfate and unreacted ions. The collected material was dried overnight at 80°C in a convection oven and subsequently ground to a fine powder using a mortar and pestle. Calcination was performed in an alumina crucible using a programmable muffle furnace with a heating rate of 30°C/min to 600°C, maintained for 2 hours, and then allowed to cool naturally to room temperature.

Characterization

Fourier Transform Infrared (FTIR) spectroscopy was performed using a benchtop Cary 630 FTIR by Agilent to monitor the chemical transformation from precursor to oxide and to confirm the removal of sulfate groups. Field Emission Scanning Electron Microscopy (FE-SEM) of GeminiSEM-500 by Carl Zeiss coupled with Energy Dispersive X-ray Spectroscopy (EDS) of XMax-80 by Oxford Instruments was used to examine particle morphology, size distribution, and elemental composition. Samples for FESEM analysis were prepared by mounting powder on carbon-coated stubs, followed by sputter-coating with a thin conductive layer to prevent charging. X-Ray Diffraction (XRD) was employed to confirm the formation of CeO_2 and to evaluate its crystallinity used to determine the CeO_2 formation and its crystallinity.

RESULTS AND DISCUSSIONS

Formation of cerium oxide powder

Figure 1 shows the physical appearance of the cerium compounds before and after calcination, synthesized via the sonication-assisted precipitation of cerium hydroxide-sulfate. A distinct colour change is observed, from dark yellow in the precipitate to pale yellow in the post-calcination powder.

(a) (b) (c)

Figure 1: Cerium compounds; a) Precipitated cerium sulfate hydroxide after sonication; b) dried precipitate cerium sulfate hydroxide before calcining; c) post calcination powder.

FTIR Analysis

FTIR spectroscopy was employed to characterize the cerium(IV) sulfate hydrate, and the precipitated cerium hydroxide-sulfate both before and after calcination by identifying the chemical bonds and functional groups present. The FTIR spectra of the three samples are shown in Figure 2. A broad band centered around 3398 cm^{-1} was attributed to the O-H stretching vibrations of both adsorbed water and surface hydroxyl groups present in all samples. Another band around 1640 cm^{-1} related to the H-O-H bending mode were also observed in all samples. The stretching band is particularly broad due to the complex interactions between water molecules via hydrogen bonds.

The sulfate ion ($SO4^{2-}$) exhibits several characteristic infrared (IR) absorption bands associated with its vibrational modes. The consistent absorption observed around 1300-1400 cm^{-1} across all samples is attributed to sulfate (SO_4^{2-}) vibrations. In cerium(IV) sulfate hydrate, these bands typically appear in the asymmetric stretching (ν_3) around 1100 cm^{-1}, while the precipitated sample before calcination shows an intense absorption peak at around 1058.6 cm^{-1} corresponding to the symmetric (ν_1) stretching modes of sulfate anions respectively coordinated to Ce^{3+}, indicating well-defined Ce-OSO_3 linkages within the precursor matrix (Colthup et al., 1990). Two weak shoulders appeared around 1136.8 cm^{-1} and 993 cm^{-1} corresponded to the asymmetric (ν_3) and combination or overtone modes of the sulfate group or bending vibrations of hydroxylated sulfate species respectively (Colthup et al., 1990, Smith , 2011). These two peaks confirm the coexistence of oxyhydroxide and sulfate species after precipitation, suggesting that the treatment of cerium (IV) sulfate hydrate with ammoniuma hydroxide led to the formation of cerium hydroxide. Notably, the increased intensity and resolution of the IR bands following NH_4OH treatment indicate the formation of more well-defined chemical bonds, suggesting a fundamental rearrangement of the cerium compound's precursor structure. This structural modification correlates with the development of nanoporous particles observed via FESEM (Figure 3) and the enhanced crystallinity evidenced by XRD analysis (Figure 5).

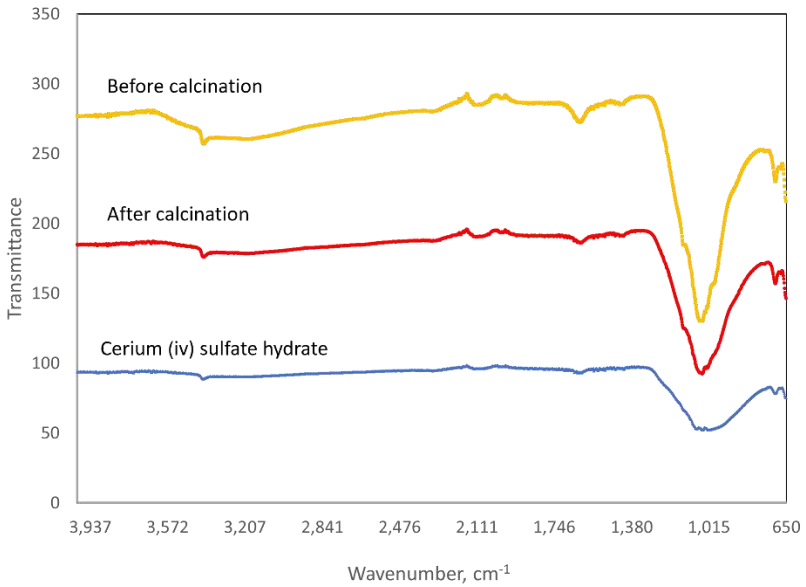

Figure 2: FTIR spectra of cerium sulfate (IV) hydrate as precursor, precipitate cerium suflate hydroxide before and after calcination

Following calcination at 600°C, significant changes were observed in the FTIR spectrum of the calcined sample (Figure 2). The broad O-H stretching band was substantially reduced, indicating dehydration of the material upon calcination. The disappearance of the sulfate bands at 993 cm^{-1}, confirms the successful removal of sulfate groups through thermal decomposition. The reduced intensity of other peaks between 1600 – 2800 cm^{-1} confirms minimal organic or carbonate contamination. The appearance of bands at 1643, 1555 and 1405 cm^{-1} referring to absorption of atmospheric carbon dioxide which nearly disappeared after calcination (Ramjeyanthi et al., 2019). A weak shoulder near 701 cm^{-1} can be attributed to Ce–O–H bending or lattice M–O vibrations, indicating the development of a metal–oxygen framework within the precursor (Colthup et al, 1990, Smith, 2011). According to Ramjeyanthi et al., 2019, absorption bands appearing below 800 cm^{-1} represents the metal-oxygen stretching (Ce-O stretch) which confirms the formation of CeO_2 particles. The presence of an intermediate-intensity spectrum suggests partial structural modification of the powder after calcination at 600 °C, while some characteristics of cerium sulfate are still retained.

Morphological Characterization

FE-SEM analysis in Figure 3 reveals distinct morphological differences among the precursor, the precipitate material before, and the calcined sample. The precursor shows irregular shape particles that are heavily agglomerated (Figure 3a) and exhibits a dense morphology (Figure 3b). In contrast, the precipitated cerium sulfate hydroxide displays more regularly shaped particles with reduced agglomeration (Figure 3c) and the presence of
porous structures on the particle surfaces (Figure 3d). Figure 3d and 3e compare the morphologies of the precipitated and post-calcination powders, respectively, demonstrating that calcination at 600 °C enhances the development of porosity. Figure 3f conforms that calcination transforms the precipitate into a nanoporous structure with a more uniform particle distribution. The size of the CeO_2 powders were in nano-range, however the specific size was not determined in this study.

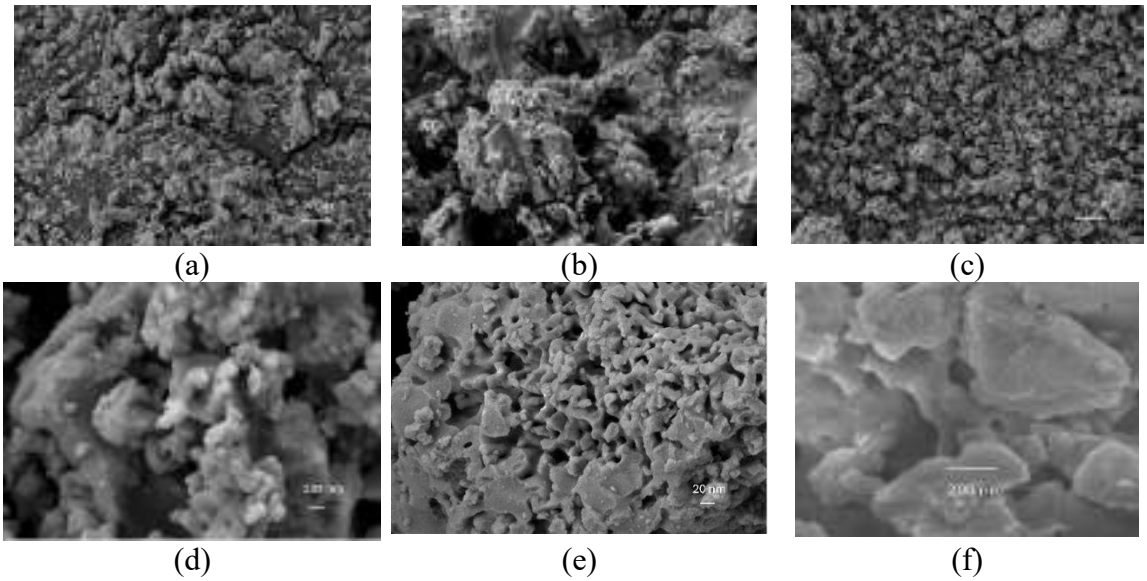

Figure 3: Surface morphology of cerium compound; (a) precursor shows irregular shape particles, (b) precursor exhibits dense structure, (c) precipitate has regular shape particles, (d) precipitate displays combination of dense and porous structure, (e) post-calcination precipitate has more obvious porous structure, (f) close-up image of uniform nano-sized CeO_2 powders with nanoporous structure after calcination.

Elemental analysis

Figure 4a shows the EDX spectrum for post-calcination precipitate, confirming that the powder contains only three elements which are Ce, O and S. Table 1 presents that the cerium content increases from 38.05 wt.% in the precursor to 64.3 wt.% in the post-calcination powder. Post-calcination analysis demonstrated that the sulfur was not eliminated completely, suggesting the crystallization process during precipitation is not sufficient. Longer ageing times may be required to enhance crystallization and promote further sulfur removal, and additional thermal treatment studies are necessary to evaluate the effectiveness of heat treatment in producing near–high-purity CeO_2.

Table 1: Elemental composition of precursor, precipitate before calcination and post-calcination.

Element	Samples / concentration (Wt.% ± Wt.% sigma)		
	CeSO4	Precipitate before calcination	Precipitate after calcination
Cerium (Ce)	38.05 (± 0.14)	55.29 (±0.26)	64.3 (±0.25)
Sulfur (S)	15.54 (± 0.07)	11.56 (±0.09)	10.75 (±0.12)
Oxygen (O)	46.41 (± 0.14)	33.16 (±0.20)	24.95 (±0.22)

Phase composition analysis

Figure 4 displays the XRD patterns of the precursor and the post-calcination precipitate. The patterns indicate the crystallinity of the post-calcination precipitate increases, confirming that the precursor is cerium (IV) sulfate hydrate, while the post calcined precipitate is CeO_2. The major diffraction peaks (2 theta) for CeO_2 could be indexed and lattice at 28.59° (111), 33.03° (200), 47.59° (220) and 56.36° (311), 69.62° (400) and 76.72° (331). The major diffraction peaks (2θ) for CeO_2 are observed at 28.59° (111), 33.03° (200), 47.59° (220), 56.36° (311), 69.62° (400), and 76.72° (331), consistent with previous reports (Malatesh et al., 2017). These results suggest that further thermal treatment may be necessary to enhance the crystallinity of CeO_2 and achieve a higher-purity product.

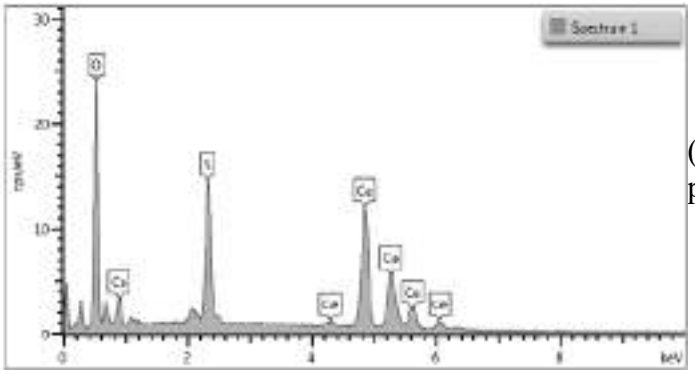

(a) EDS spectrum for post calcination powder

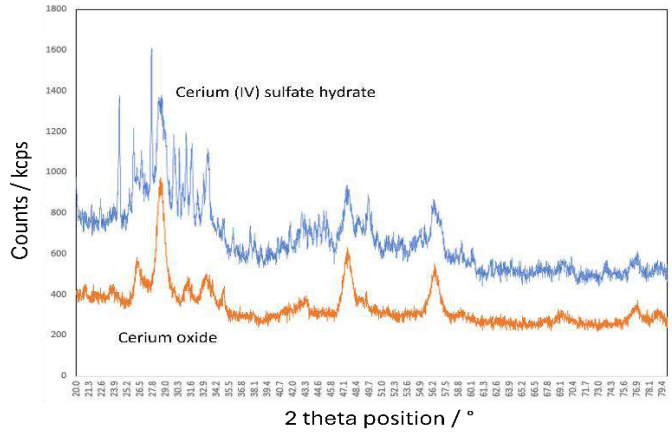

(b) XRD spectra for precursor, precipitate before and after calcining

Figure 4: (a) Elemental composition of the post-calcination powder, and (b) XRD patterns showing the phase composition of the precursor, precipitate before calcination, and post-calcination powder

Mass Balance and Yield Analysis

The yield of the precipitated powder, measured before and after calcination, indicated 85% mass retention following thermal treatment. The 15% mass loss is attributed to the removal of structural water and the decomposition of sulfate groups into volatile species (H_2O, SO_2, O_2). This observed yield consistent with the theoretical mass loss expected from the dehydration and desulfation reactions during calcination.

CONCLUSION

A simple and efficient precipitation-calcination method was successfully employed to synthesize CeO_2 from cerium (IV) sulfate hydrate. FTIR analysis confirmed the conversion of the hydroxide-sulfate precursor to CeO_2, evidenced by the disappearance of sulfate bands and emergence of characteristic Ce-O vibrations. FESEM-EDX analysis revealed the formation of nanoporous CeO_2 structures with uniform morphology and confirmed the elemental the purity of Ce, while XRD analysis confirmed the oxide phase formation and the crystallinity. The synthesis achieved 85% mass retention, demonstrating the efficiency of this route for CeO_2 production. The scalability and simplicity of this method make it attractive for industrial scale-production of high-quality CeO_2 nanoparticles. Future work will focus on optimizing calcination parameters to further improve yield and crystallinity, as well as evaluating the biosensing and catalytic performance of the synthesized CeO_2 nanoparticles to explore their practical applications.

REFERENCES

Alifanti, M., Baps B., Blangenois N., Naud J., Grange P., and Delmon B. (2003), Characterization of CeO2-ZrO2 Mixed oxides. Comparison of the citrate and sol-gel precipitation method. *Chemical Material*, 15 (2): 395. https://doi.org/10.1021/cm021274j

Bojana S, Zeljka A., Nadica A., Randeka K., Miodrag Mitric, Amelia M. and Miroslav D.D., (2008), Combustion synthesis and characterization of CeO2 Nanopowder, *Acta Chimica Slovenica*, 55: 486. https://vinar.vin.bg.ac.rs/handle/123456789/3545

Campbell, C. T. and Peden, C.H. F., (2005), Oxygen vacancies and catalysis on ceria surfaces. *Science*, 309 (5735): 713-714. https://doi.org/10.1126/science.1113955

Colthup, N.B., Daly, L.H. and Wiberley, S.E., (1990), Introduction to Infrared and Raman Spectroscopy (3rd ed.). Academic Press

Dahle, J. and Arai, Y., (2015), Environmental Geochemistry of Cerium: Applications and toxicology of cerium oxide nanoparticles. *International Journal of Environmental Research and Public Health*, 12 (2): 1253. https://doi.org/10.3390/ijerph120201253

Das, S., Dowding, J.M., Klump, K.E., McGinnis, J.F., Self, W. and Seal, S., (2013), Cerium oxide nanoparticles: Applications and prospects in nanomedicine, *Nanomedicine*, 3(3): 313. https://doi.org/10.2217/nnm.13.133

Gupta, C.K. and Krishnamurthy, N., (2005), Extractive Metallurgy of Rare Earths, CRC Press.

Krystof Skrbek and Ondrej Jankosvsky, (2019), Synthesis and characterization of ceria nanoparticles, *AiP Conference Proceedings,* 2170: 020018. https://doi.org/10.1063/1.5132737

Mahmoud A., Hussein, Ajahar Khan, and Khalid A. Alamry, (2022), A highly efficient electrochemical sensor containing polyaniline/cerium oxide nanocomposites for hydrogen peroxide detection. *RSC Advance*,12: 31506. https://doi.org/10.1039/D2RA05041B

Pujar, M.S., Hunagund, S.M., Desai, V.R, Patil, S. and Sidarai A. H., (2017), One-step synthesis and characterizations of cerium oxide nanoparticles in an ambient temperature via co-precipitation method. *AIP Conference Proceedings*, 1942: 050026-1. https://doi.org/10.1063/1.5028657

Phokha, S., Pinitsoontorn, S., Chirawatkul P., Poo-arporn Y. and Maensiri. S., (2012), Synthesis characterization and magnetic properties of monodisperse CeO2 nanospeheres prepared by PVP-assisted hydrothermal method. *Nanoscale Research Letters*, 7: 425. https://doi.org/10.1186/1556-276X-7-425

Pouretedal, H.R. and Kadkhodaie, A., (2010), Synthetic CeO2 nanoparticle catalysis of methylene blue photodegradation: kinetics and mechanism. *Chinese Journal of Catalyst*, 3 (11-12): 1328.
https://doi.org/10.1016/S1872-2067(10)60121-0

Ramjeyanthi, N., Alagar, M. and Muthuraman, D., (2019), Effect of calcination temperature on the structural and optical properties of Synthesised ceria nanoparticles via chemical method, *Journal of Applied Science and computations*, 5(9): 577.
ISSN Number: 1076-5131

Smith B.C., (2011), Fundamentals of Fourier Transform Infrared Spectroscopy (2nd ed.). CRC Press.

Sun, C., Li, H. and Chen, L., (2012), Nanostructured ceria-based materials: Synthesis, properties, and applications, *Energy & Environmental Science*, 5(9): 8475-8505.
https://doi.org/10.1039/C2EE22310D

Wang, H., Jian, M., Fan, J., He, Y. and Wang, Z., (2024), Scalable synthesis of Au@CeO_2 nanozyme for development of colorimetric lateral flow immunochromatographic assay, *Talanta*, 273: 125852.
https://doi.org/10.1016/j.talanta.2024.125852

Wang Y., Mori T., Li J. and Ikegami T., (2002), Lo temperature synthesis of praseodymium-ceria nanopowders. *Journal of American Ceramic Society*, 85: 3105.
https://doi.org/10.1111/j.1151.2916.2002.tb00591

Zhanxiao-Lu, Yarong Cheng, Zhang Y., Xuefeng Wang and Pengcheng Xu, (2021), Non-enzymatic free bilirubin electrochemical sensor based on ceria nanocube. *Sensors and Actuators: B. Chemical*, 329: 129224
https://doi.org/10.1016/j.snb.2020.2002.129224